Journal of Materials Chemistry C

Embedded Optical Nanosensors for Monitoring the Processing and Performance of Polymer Matrix Composites

Journal:	*Journal of Materials Chemistry C*
Manuscript ID	TC-REV-06-2019-003118.R2
Article Type:	Review Article
Date Submitted by the Author:	28-Oct-2019
Complete List of Authors:	Lioi, David; Universal Technology Corporation, Materials and Manufacturing; Air Force Research Laboratory Materials and Manufacturing Directorate, Materials and Manufacturing Directorate Varshney, Vikas; Air Force Research Laboratory Materials and Manufacturing Directorate, Materials and Manufacturing Directorate Izor, Sarah; UES Inc, Materials and Processes; Air Force Research Laboratory Materials and Manufacturing Directorate, Materials and Manufacturing Directorate Neher, Gregory; Universal Technology Corporation, Materials and Manufacturing; Air Force Research Laboratory Materials and Manufacturing Directorate, Materials and Manufacturing Directorate Kennedy, William; Air Force Research Laboratory Materials and Manufacturing Directorate, Materials and Manufacturing Directorate

Journal Name

ARTICLE TYPE

Cite this: DOI: 10.1039/xxxxxxxxxx

Embedded Optical Nanosensors for Monitoring the Processing and Performance of Polymer Matrix Composites

David B. Lioi,[ab] Vikas Varshney,[a] Sarah Izor,[ac] Gregory Neher,[ab] and W. Joshua Kennedy*[a]

Received Date
Accepted Date

DOI: 10.1039/xxxxxxxxxx

www.rsc.org/journalname

The performance of polymer matrix composite (PMC) materials relies on the history of chemical and physical environments to which they have been subjected. The understanding of a PMC's current state is crucial in order to optimize processing parameters and thereby maximize material performance. Nanoscale embedded sensors (such as colloidal nanoparticles, quantum dots, and molecular compounds) provide a non-destructive, *in-situ* platform to monitor material properties through the utilization of the nanosensors' optical response and corresponding modulation thereof through interactions with the environment. This review summarizes the current state of embedded plasmonic and photoluminescent optical sensing pertaining to local chemical environment, temperature, viscosity and stress/strain as applicable to PMCs. We highlight important scientific advances that have enabled new sensing approaches and emphasize promising directions where advances are still required.

1 Introduction

Nanoscale materials, in the form of nanoparticles or molecular species, are often added to polymers to form nanocomposites with new or improved functionality.[1–7] Nanosensors are a subclass of nanomaterials that are sensitive in some way to their local environment, and thereby allow for the detection of key properties of the material or its surroundings at sub-micron length scales. Nanocomposites with integrated sensing collectively comprise one sub-class of so-called "smart materials" with broad interest and potential applications. Among various nanosensing mechanisms, optical nanosensors rely on changes in the optical properties such as absorption, scattering, or photoluminescence in response to changes in the surrounding materials' state. These are of particular usefulness when the host matrix is translucent because the sensor readout does not require additional electrical contacts or other modifications to the material.

Given the widespread relevance of optical nanosensors in smart materials, there have been many excellent reviews focusing on specific molecular and nanoparticle architectures or on specific sensing capabilities.[8–11] However, the application of these emerging technologies to modern structural materials is still underexplored. In particular, polymer matrix composites (PMCs) are increasingly used in the aerospace, automotive, and sporting goods industries where a high strength-to-weight ratio is desired. In their formulation, processing, and manufacturing, as well as during their operational use, PMCs are subjected to a wide range of temperature, pressure, stress, and strain, during which they undergo large changes in chemical state and mechanical properties.

Over the course of a typical manufacturing process, small variations in the condition of the starting material can result in large variations in residual stresses and degree of cure in the final part. In real manufacturing environments (e.g., inside a pressure mold or autoclave in the case of aerospace grade composites) it is difficult or impossible to assess the temperature and cure state of the PMC in real time. Parts that are rejected because of dimensional tolerances or internal flaws are a major driver of cost for PMCs, especially in the aerospace industry.[12] During service, the mechanical properties of a PMC can change dramatically due to moisture uptake, physical aging, and thermo-oxidative degradation, even when there are no detectable cracks in the part. Because of this, existing strategies for structural health monitoring and material state awareness in PMCs are much less robust and reliable than in other structural materials.[13]

Ultimately, the mechanical performance of a PMC is related to its specific thermo-chemo-mechanical history. Thus, direct sens-

[a] *Materials and Manufacturing Directorate, Air Force Research Laboratory, Wright-Patterson Air Force Base, Ohio 45433, United States. E-mail: william.kennedy.21@us.af.mil*
[b] *Universal Technology Corporation, Beavercreek, Ohio 45432, United States.*
[c] *UES Inc., Beavercreek, Ohio 45432, United States.*

† Electronic Supplementary Information (ESI) available: [details of any supplementary information available should be included here]. See DOI: 10.1039/b000000x/

ing of material state parameters can enable better control systems for manufacturing and more reliable material state awareness. In particular, the ability to sense properties such as temperature, viscosity, stress, and strain *inside* a polymer can provide vital information during material processing and use. These quantities relate the chemical state (eg, crosslink density, degradation), chain entanglement, and free volume of polymers to the bulk material properties that determine their performance in structural applications. The ability to sense these quantities is critical, not only to effectively control process parameters, but also to optimize performance during use. Table 1 illustrates the importance of these properties in various process environments.

The potential for optical nanosensors to detect these properties on the interior of a PMC with high spatial resolution makes them attractive for further development. However, there are significant challenges in designing optical nanosensors that can operate over the entire range of thermomechanical conditions experienced by these materials. For example, during the manufacture of a typical aerospace grade, carbon fiber reinforced bismaleimide composite the temperature can range from 20-250 °C, the viscosity can range from 10-10^9 cPs, and the local residual stresses from cure shrinkage and thermal expansion can reach several hundred MPa [12]. In this review, we summarize the state of the field of optical nanosensing with regards to structural polymers, with an eye toward sensing the local properties during their manufacturing, processing, and/or their lifetime in the field, up to and including exposure to extreme conditions. We highlight the scientific advances that have contributed to the current state of the art, and we identify key remaining challenges in designing, synthesizing, and characterizing optical nanosensors for use in structural polymer matrix composites.

In designing an optical nanoparticle sensor there are three factors that impact its effectiveness:

1. The degree of coupling of the sensor to a given material parameter in the surrounding matrix.

2. Whether the sensor response is due to internal material parameters (*dielectric function*) or geometric parameters (*particle shape/clustering*).

3. The mechanism used to readout the gathered information from the sensor.

In this review, we focus on plasmonic and photoluminescent mechanisms (factor 3) and review strategies to address (factors 1 and 2) with regard to each individual material property of interest (temperature, viscosity, etc.) and the various types of sensors employed to this end. We also comment on the limitations/challenges of these strategies associated with sensitivity and/or specificity wherever applicable. We conclude this review by summarizing the disparities between current sensing capabilities of nanoparticles and the needs as pertains to modern structural polymeric materials during their processing and performance.

2 Background

In this section, we will give a brief, applied background into optical sensing via plasmonic resonances and photoluminescence in order to contextualize the current state-of-the-art approaches to material property sensing. A simple yet important differentiation between these two sensing mechanisms is that the former phenomenon can be found primarily in materials with metal-like electronic band structures (or materials with free electrons) and the latter is found primarily in those with semiconducting or insulating band structures.

2.1 Plasmonics

In the case of plasmonic optical sensing, it is the coupling of conduction electrons with photons at the surface of a metal that gives rise to the optical response. The geometry of the metal surface (particle shape), the dielectric constant of the material (matrix) in contact with the metal, and the proximity of particles to each other, each play an important role in tuning the energy of the plasmonic resonance. Designing a plasmonic sensor relies on understanding how material parameters in the external matrix (*temperature, stress/strain, etc.*) couple to and affect each of these phenomena.

The metal: The response of charge carriers in a metal to an external electromagnetic field may be described by the frequency-dependent complex dielectric constant. The dielectric constant depends on material parameters such as atomic spacing, electron scattering, and carrier density, which can each change with temperature, pressure, and defect density. Typical nanoparticle systems utilize noble metals such as silver or gold for their relative inertness to chemical environments (especially in the case of gold) and high free-electron density. Additionally, silver and gold have interband transitions that give rise to localized surface plasmon resonances in the visible spectrum.

The matrix (dielectric medium): In the context of this review, the matrix is the material whose properties are being sensed. Thus, for a practical sensor system, the imaginary part of the matrix's dielectric constant is near zero. Matrices with significant imaginary dielectric values are not suitable for plasmonic sensors due to signal loss and complexities in calculating the plasmonic response. In the context of this review, most structural polymers are transparent over broad spectral regions in the visible and near infrared. Thus, they are well suited for plasmonic sensing applications.

As with metals, the dielectric of the matrix changes with temperature, pressure, and chemical bonds. In the case of a heterogeneous matrix, the components that are sensed plasmonically must be near the metal-dielectric interface. For example, a distribution of plasmonic nanoparticles in a polymer matrix can give information only on local (near metal-matrix interface) temperature, degree of cure, and other material parameters. Thus, the matrix properties can be mapped with high spatial resolution due to the locality of the nanoparticle sensor.

The geometry: The oscillations of free electrons confined to the metal-matrix interface is called a localized surface plasmon (LSP). The dispersion of LSP energies with respect to geometry

Sensing	Intrinsic Material State Properties	Process Parameters	Performance Factors
Chemistry	Cross-link Density Oxidation Decomposition	Degree of Cure	Degradation
Temperature	Glass Transition Melting Point Reaction Rates	Cure Kinetics	Thermal Expansion Thermal Stresses
Viscosity	Chain Mobility Reptation	Mold Filling Void Formation/Migration 3D Printability	Creep Embrittlement
Stress/Strain	Residual Stress	Cure Shrinkage Spring-In	Crack Initiation/Propagation Mechanical Failure

Table 1 Quantities of interest for sensing in polymer matrix composites are listed along with relevant intrinsic material properties and macroscopic composite characteristics that are important during processing and performance.

for two different matrix dielectric constants are shown in Fig 1a. The role of increasing nanoparticle size is to decrease the energy of the observed optical resonance and vice versa. The steepness (as well as other fine structure features not shown) of the dispersion depends on the dielectric constants of the metal and matrix. Resonance energies are highly sensitive to the matrix dielectric constant, and they are more sensitive to particle size when the particle is surrounded by a matrix with a low dielectric constant.

The nanoparticle geometry also affects the resonant mode shapes where the electric field associated with the resonant modes extends beyond the particle-matrix surface. This can be illustrated by visualizing the electric field associated with three degenerate LSP modes for a spherical nanoparticle that lie along the x, y, and z axes as in Fig 1b. In the case of a nanorod, broken symmetry results in an additional non-degenerate longitudinal mode that is largely decoupled from the doubly degenerate transverse mode. Thus, physical processes that changes the shape of these nanoparticles also change the observed LSP energies. Furthermore, these different modes typically have different sensitivities to changes in the metal, matrix, or geometry, which potentially allows anisotropic particles to act as multimodal sensors.

LSP-LSP coupling: Because the fields associated with these resonances extend beyond the particle surface, plasmonic modes can couple to each other when particles are close together as shown in Fig 1b. This allows for sensing strategies that rely on changes in interparticle distances. The sensitivity of coupling approaches depends largely on the spatial extent of these modes.

In summary, plasmonic nanoparticles have optical resonances that are sensitive to changes in the local environment through their dependence on dielectric constant, geometry, and interparticle coupling. These features enable many promising approaches in developing optical nanosensors for material properties.

2.2 Photoluminescence

Photoluminescence occurs in a three-step sequence. First, in the photoexcitation event, a material absorbs photons to promote ground-state electrons to an excited electronic state. Next, excited electrons may relax through several phonon excited states as surplus energy dissipates via non-radiative mechanisms. Finally, energized electrons spontaneously de-excite to reoccupy the electronic ground state and lower energy photons are re-emitted. With respect to optical sensing, the excited-state lifetime, emission intensity, and energy of luminescent photons are measurable features that can change as a result of interactions with the environment. Photoluminescence quantum efficiency (PLQE) is the ratio of the number of emitted photons to the number of absorbed photons. This is related to the excited-state lifetime, which is a measure of the average time that a system remains in an excited state before photon emission. Both quantum efficiency and the excited-state lifetime are impacted by changes in radiative (modifications to the lattice spacing, destruction of transition pathway) and/or non-radiative (rotational degrees of freedom, thermal bath, etc.) processes. Thus, in most cases, changes in in PL emission are phenomenologically related to changes in inter-band transitions and non-radiative decay.

Inter-band transitions: Changes in radiative photon energy are generally indicative of some restructuring of the overall lattice, which may be brought about either by environmental factors or discrete external stimuli. Such is the basis, for example, of stress/strain sensing in fluorescent tetrapod quantum dots (see Fig. 2). Under mechanical influence, physical deformation of the overall tetrapod architecture alters the inter-band transition energy of the core quantum dot.

Non-radiative decay: Non-radiative decay can occur through several mechanisms (vibration-driven collisions, intersystem-crossing, energy transfer) and ultimately serves as the foundation for several photoluminescent sensing modalities as environmental factors (temperature, pressure, etc.) can influence the rate of non-radiative decay. For instance, photoluminescent molecular

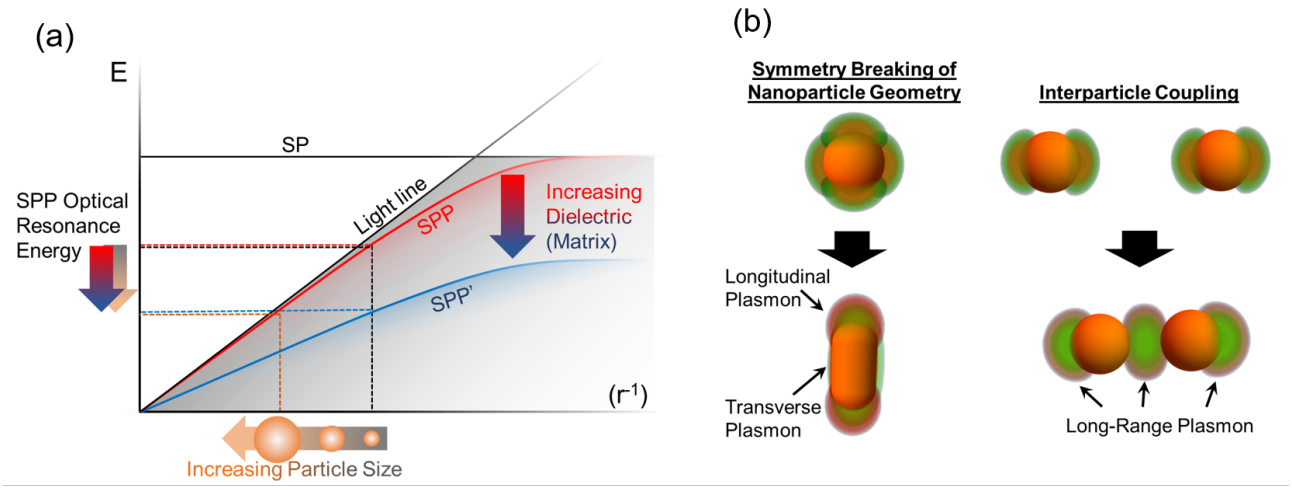

Fig. 1 (a) Dispersion diagram showing energy vs reciprocal space of the surface plasmon frequency and its coupling with the light line to produce surface plasmon polaritons (SSPs) for different metal dielectric interfaces. In the case of localized surface plasmons (LSPs) the particle size and geometry influences the allowed energy of the resonance by determining the size of the plasmon modes. (b) These LSP energies are degenerate for a sphere, but can be tuned by breaking the symmetry as in the case of rods. Processes that change the shape of the particle will also change the observed energy resonances of the plasmonic modes. Bringing particles to close proximity with each other leads to coupling of the plasmonic modes which will also modify the observed energy resonance of the plasmonic modes.

rotors are powered by the energy of absorbed photons where the rotation is sensitive to changes in the surrounding viscosity. As molecular rotation meets mechanical resistance in a highly viscous environment, non-radiative decay channels, originally funneled into molecular motion, become obstructed. Similarly, increased temperatures promote non-radiative recombination of excited-state electrons with electronic holes in the ground state, decreasing quantum yield. Variations in non-radiative discharge brought about by environmental changes will ultimately determine the energy, timescale, and number of photons available for the ensuing radiative emission, thereby providing opportunities to sense a number of external environmental factors.

Each of the phenomena discussed in this section (plasmonic resonances and photoluminescence) may be used to design an optical nanosensor based on the interaction of the underlying optical mechanisms with the material parameter of interest. For the remainder of this review we describe various strategies for using these specific interactions to measure local chemistry, temperature, viscosity, and stress/strain in a matrix material of interest.

3 Nanosensors of local chemical environment

The need for local chemical sensing in structural composites lies in the desire to monitor the state of chemical reactions at local regions, both during processing (e.g., curing reactions) and performance (e.g., oxidative degradation). In composite materials, the dielectric surrounding medium is either a liquid-like polymer matrix in its pre-cure state, or the solid phase post-cure matrix. However, to date, the literature have predominantly been focused at the chemical sensing phenomenon in the liquid state. Hence, this section of the review at best is applicable for sensing in pre-cure matrices (in their liquid form) and is otherwise meant to provide context for future work and opportunities in solid matrix chemical sensing. The reported literature discussed below therefore focuses on chemical sensing in the liquid phase and cover the state of the art for optical chemical sensing and recent solutions in using nanoparticles as chemical sensors. Specific attention is given towards strategies used in creating either a robust or a multimodal sensor.

The plasmonic/photoluminescent optical response of a nanoparticle to its local environment permits sensitivity to nearby chemical species in one of two ways: The first, by virtue of the dielectric provided by the nearby chemical species (plasmonic), and the second, by providing alternate (or modifying existing) decay channels that could either quench or enhance photoluminescence [14].

A key challenge in using the plasmonic mechanism is the lack of specificity. The nanoparticle is sensitive to all of the local dielectric species near the nanoparticle and not just the ones that are desired for a given application. An additional selection mechanism is often required if the nanoparticle is to be robust in an uncontrolled environment. Tang et al. [15] approached this problem in developing a nanosensor for detecting prostate-specific antigen (PSA). Their solution was to deposit a silver shell on the surface of the gold nanorod (Au-NR) dimers. The dimer geometry gave rise to circular dichroism plasmonic resonance which can be subsequently monitored in the presence of the PSA. The PSA also has a circular dichroic optical response, making this sensing scheme robust against other chemical agents within the matrix which do not possess circular dichroism. Indeed, this particular nanoparticle is one of several produced by this group, including gold nanoparticle pyramids which were used for endonuclease analysis [16] and a chiral pyramidal sensor which was used to detect DNA [17] (shown in Fig. 3b). The silver coating on the dimers were found to experimentally have the added benefit of enhancing the observed signal. Other examples include coating silver nanoparticles with

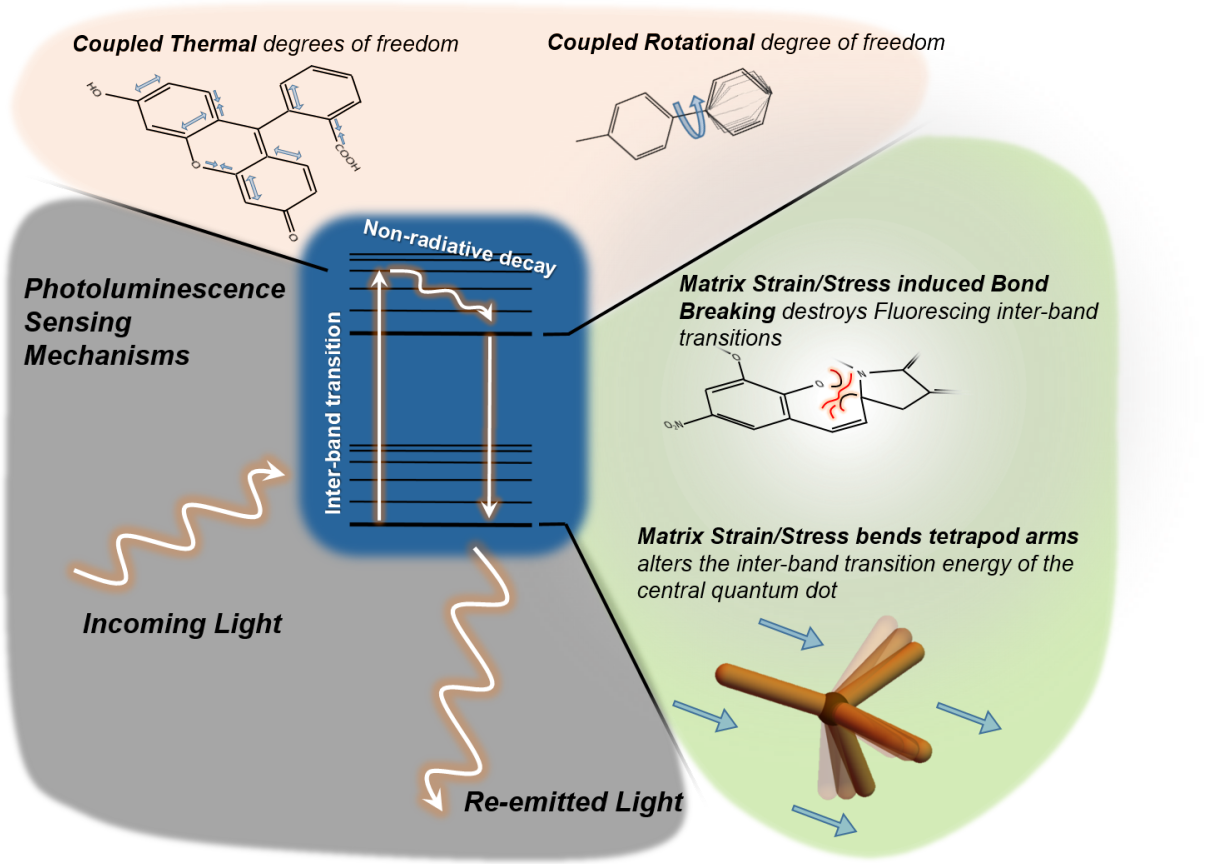

Fig. 2 Schematic representation of photoluminescence sensing mechanisms driven by changes in non-radiative decay (orange) and modifications to the inter-band transitions (green).

sulfanilic acid to detect melamine,[18] polyacrylate functionalized gold nanoparticles for selective detection of Aluminum (Al) and Flouride (F) in water,[19] and also for Lead (Pb) sensing when functionalizing with maleic acid.[20]

Another way to solve the specificity problem is to provide a nanoparticle sensor array whose signal is self-referential, i.e. one optical signature is sensitive to changes in the presence of the chemical species to be monitored while the other is not. This was accomplished by Rivero et al. with dual populations of gold and silver nanoparticles encapsulated with poly(diallylammonium chloride) (PDDA) which were used to monitor the presence of H_2O_2 in solution.[23] It was observed that the localized surface plasmon resonance (LSPR) band of the silver nanoparticles is gradually decreased in intensity whereas the LSPR of the gold nanoparticles is practically unaltered as the hydrogen peroxide molar concentration is increased, thereby utilizing the better chemical stability of gold relative to silver. This process is irreversible and therefore could be applied in situations where the evolution of time is a factor. Another method that monitors the presence of H_2O_2 in solution was developed by Sodzel et al. where it was found that the photoluminescence of ZnO nanoparticles are quenched by up to 90% at a 100 mM level of H_2O_2.[24] This process is non self-referential, but instead is reversible in the sense that the nanosensor's response does not depend on the history of the material. Rather, it is an instantaneous monitoring response as long as the nanoparticles have not degraded.

In a controlled environment, the mechanisms for sensing chemical changes can be more sophisticated. For example, changes in the plasmonic/photoluminescent response due to aggregation of nanoparticles can be used in response to the changing chemical conditions of a solution, which has been used to discriminate biothiols,[25] organophosphates,[26] thiocyanate,[22] (shown in Fig. 3d) or the determine the presence of protamine.[27] Sun et al. has used conjugated nonspecific dye-labeled DNA sequences absorbed onto gold nanoparticles. This had the benefit of not only monitoring the salt content of the solution which resulted in aggregation of the nanoparticles, but by simultaneously utilizing the fluorescent and plasmonic signals of the core-ligand structure, was also able to distinguish between the presence of different protein species in solution.[28] It is noted that the sensor platform can be generalized by altering the fluorescing DNA sequences.

All of the previously mentioned methods for chemical sensing have been implemented in solution based systems, but when tackling the problems in monitoring polymeric structural materials, such as fiber reinforced polymer matrix composites used in the aerospace and automotive industries, it is necessary to have methods that function well in solids. Indeed, there is a need to

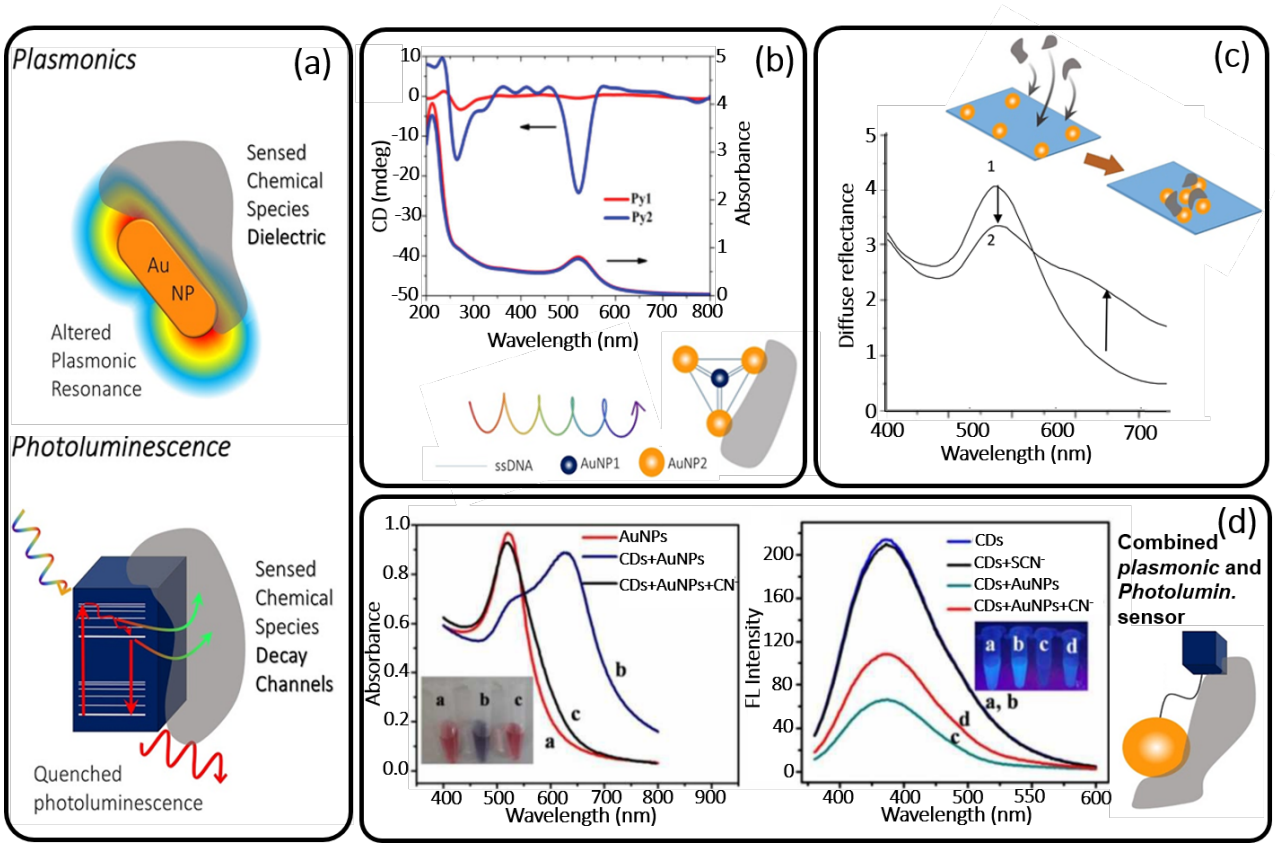

Fig. 3 (a) Illustrations of the effect of a chemical species (grey shape) locally interacting with a plasmonic nanoparticle (orange) or a photomluminescent nanoparticle (blue cube) (b) detection of DNA based on two types of selfassembled NPs pyramids. CD and UV-vis spectra of Py1 and Py2[17] (c) Diffuse reflectance of label-free gold nanoparticles on a polyurethane surface without (1) and with (2) the presence of a sensed chemical species (cysteine)[21] (d) Comparison of the nanoparticle plasmonic (left) and fluorescent (right) responses with and without the presence of a sensed chemical species[22]

monitor local chemical changes within cured thermosets such as the level of oxidation or degradation. Quality control of manufactured materials where high tolerances of local stoichiometries are required, pose a similar need in the material processing, a topic which is ripe for the application of nanoparticle sensors. In these scenarios, chemical changes could be reflected in the change in local dielectric which can be monitored plasmonically. A changing chemical environment could also modifying the probabilistic charge transfer path between donor and acceptor ions of a fluorescent nanosensor and quench or enhance the observed optical signal.

Within the literature there are few cases of nanoparticles being used in solid-phase systems in order to monitor chemical changes within the material. However, these recent efforts have mostly been used to monitor the chemical environment of liquid phases adjacent to the solid-phase sensor platform under the conditions where the solid phase remains unchanged. Examples of such solid-phase colorimetric devices have been developed by Ferhan et al.[29] by using polymer brushes as a scaffold for gold nanoparticles and Apyari et al.[21,30–32] who utilized a polyurethane foam with adsorbed gold nanoparticles. By introducing these sensor platforms into a solution, the solid-phase matrix excludes unwanted chemical species while allowing the desired ones to interact with, and be sensed by, the gold nanoparticles (shown in Fig. 3c).

Interestingly, Yang et al. developed an epoxy nanocomposite with embedded ZnO quantum dots as a casing for LED emitters.[33] Here, the function of the quantum dots is less as a sensor and more to absorb the light given off by the LED and to re-emit the light of a desired wavelength. The quantum dots themselves can be substituted to tune the re-emitted wavelength. If one were to take this system and vary different material parameters such as temperature or pressure, it would be possible to monitor the sensitivity of the nanoparticle response.

In conclusion of this section we note that there are two main concerns one must address for any nanoparticle sensor that seeks to register the chemical environment of a given matrix. The first concern is a matter of selectivity of the sensor to chemical species of interest which was extensively discussed above. The second concern was not explicitly mentioned above, but will become more apparent throughout the following sections of this review. That concern lies with the coupling of simultaneous multivariate material properties of the matrix (i.e. temperature, pressure, viscosity, and for solid matrices stress and strain) with the optical signature of the nanosensor. Thus far a major assumption (from a design perspective) inherent in the literature above is that only the chemistry of the matrix is varied while other factors such as temperature or viscosity are held constant. Sensing schemes

which directly address these other material properties are discussed in further detail in the sections below. Indeed, many of the schemes developed for temperature sensing in epoxies could be repurposed for chemical sensing and vice versa. It would be interesting to see how these nanoparticle architectures presented in this review respond to a larger material parameter phase space outside the material parameter they were designed to measure.

4 Nanosensors of local temperature

As previously described, the structural and functional composites community has a need for local chemical sensors to improve assessment of a material's cure state, structural health, or overall quality. In many of these scenarios, local temperature or temperature history are also critical for describing the integrity of a cured, aged, or damaged part. For instance, laser damage in structural composites leads to localized heating at the area of impact, yet traditional microscale thermometry cannot satisfactorily resolve the resulting temperature gradient. Such limitations emphasize the need for precise temperature sensing techniques with sub-micrometric spatial resolution. In this context, while nanoscale thermometry can be approached through a variety of techniques (infrared thermography, thermoreflectance, scanning thermal microscopy, etc.), this section directs attention to fluorescent and plasmonic sensing strategies that measure the temperature-dependent optical response of nanomaterials. Similar to chemical sensing, the interest from in temperature sensing from a materials processing perspective is predominantly driven by applications in solid or highly viscous polymer matrices. However much of the literature presented in this section stems from a biological perspective with low temperature systems (<100 °C) in soft or liquid-phase environments. Here we highlight the most common and successful strategies for high resolution optical temperature sensing, while revealing gaps in the material and temperature parameter space.

Fluorescent nanomaterials and their temperature-dependent emission spectra provide means for rapid thermal sensing with temporal resolution on the order of microseconds. In fluorescence-based thermometry, shifts in temperature alter luminescent properties, such as emission intensity, wavelength, or excited-state lifetime, of an emissive probe material. In the case of fluorescent quantum dots (QDs), two main mechanisms (thermal quenching and temperature-induced changes in lattice spacing) impact the energy and number of photons available for re-emission. First, in thermal quenching, non-radiative decay demotes excited-state electrons without photon emission to occupy electronic holes in the valence band. Increased temperatures promote such non-radiative processes which results in reduced quantum yield (QY) and overall luminescence intensity. Second, thermal modifications to the band gap energy shift the wavelength of photon emission.

Fig. 4a presents these mechanisms and exemplary data for graphene QDs in aqueous solution at biologically relevant temperatures.[34] With an increase in temperature from 10 to 80 °C, the authors demonstrated a linear decrease in fluorescence intensity and a red shift in fluorescence wavelength of almost 9 nm. Comparable thermal quenching and spectral shifts have been observed over similar temperature ranges (27 to 47 °C) for QDs in mitochondria[35] and over a broader temperature range (30 to 200 °C) for CdSe/ZnS QD thin films.[36] Considering instead a polymeric matrix, Sung et al. investigated the temperature-dependent fluorescence of CdSe-SiO_2 core-shell nanoparticles when embedded in a sol-gel material.[37] The authors found an exponential decrease in fluorescence intensity and a red shift of ~0.095 nm/°C in peak emission wavelength over 30 to 100 °C.

When properly calibrated for a given system, fluctuations in a material's fluorescence intensity can provide a straightforward observable for thermal sensing. However, absolute intensity measurements depend heavily on factors such as particle concentration, matrix material, illumination source, and detector, and ultimately lacks self-calibration when providing quantitative temperature information.[40] To overcome these hurdles, photoluminescence (PL) lifetime and ratiometric fluorescence measurements offer more robust alternatives. Regarding the former, PL lifetime is intrinsic to the material of interest and therefore eliminates sensitivity to features like concentration, matrix absorption, and excitation intensity. The typical decrease in PL lifetime at higher temperatures is another manifestation of thermal quenching as non-radiative processes increase at higher temperatures. Kalytchuk et al. examined the temperature-responsive PL lifetime of carbon dots (CDs) over various physiological temperature ranges (up to 80 °C) in water, phosphate-buffered saline, synthetic cell culture medium, and human cervical cancer cells (see Fig. 4b).[38] This group demonstrated exceptional stability and resiliency of the CDs as the PL lifetime response was stable for at least 40 h of continuous photoexcitation over a range of CD concentrations, solution pH values, and ionic strengths. Moreover, the PL lifetimes were fully reversible over cyclic temperature experiments between 15 and 45 °C. Similar intracellular sensing with comparable stability has been performed using PL lifetime measurements for Au nanoclusters.[41] Contrary to semiconductor QDs, no change in inter-band transition was observed in the CD or Au system and therefore fluorescence wavelengths remained constant.

Ratiometric, or self-referencing, fluorescence also resolves some of the issues that arise from absolute fluorescence intensity measurements. In this case, dual-emitting sensors, from one or multiple fluorescent species, exhibit two excited luminescent states. Temperature variations impact one or both photoluminescence intensities, and the fluorescence intensity ratio (FIR) describes the thermal change. Absolute temperature can then be ascertained from a single emission spectrum regardless of sample inhomogeneities, concentration, illumination source, or detector.

Nanocrystals doped with trivalent lanthanide ions (Ln^{3+}) are common dual-emitting systems leveraged for nanoscale temperature sensing. In fact, this area of research has recently gained great momentum and many excellent reviews on this topic alone have been previously published.[46–48] Lanthanide ions house strongly shielded valence-shell *f* electrons which afford multiple *f-f* excited states. Consequently, lanthanides often exhibit luminescence in multiple excited states that are viable for FIR sensing. Fig. 4c schematicizes lanthanide dual-emitting photoluminescence. Here, two adjacent thermally coupled energy levels (TCLs) experience temperature-dependent fluctuations in popula-

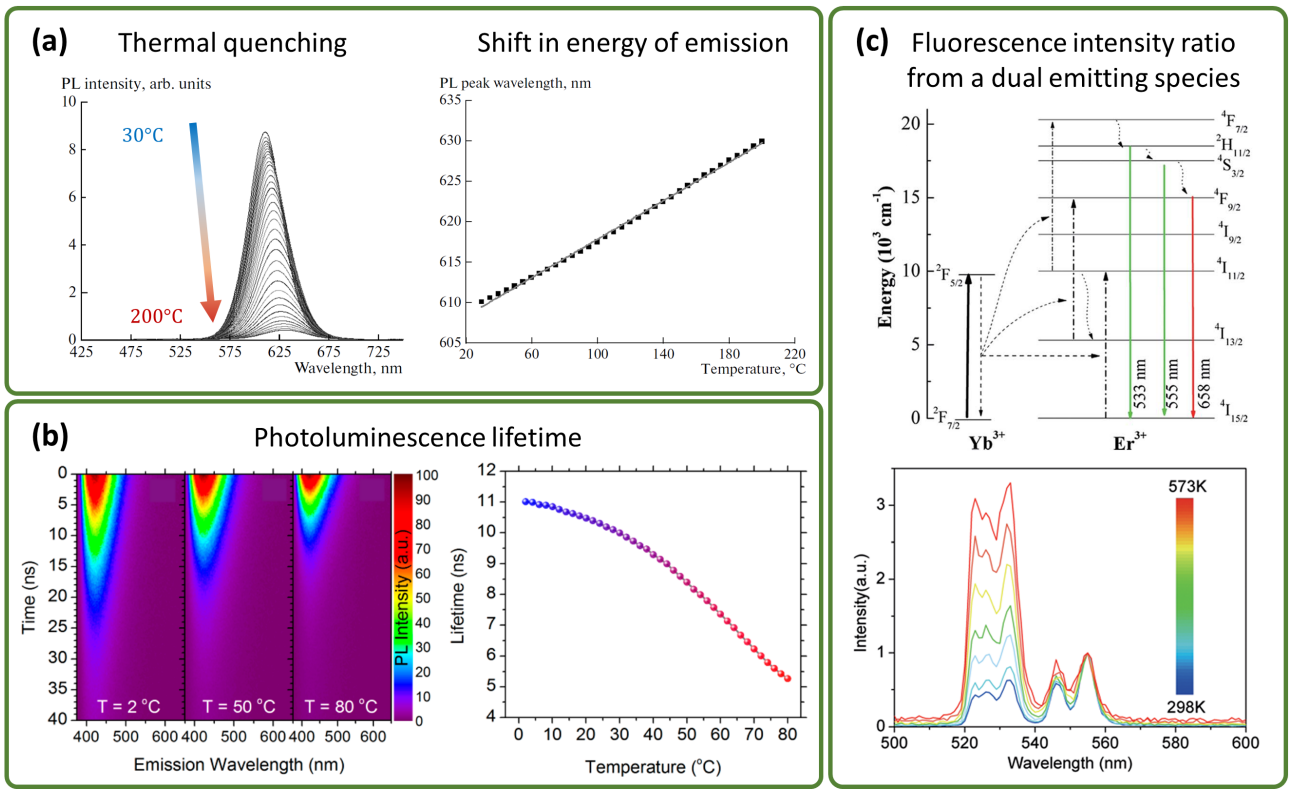

Fig. 4 (a)PL spectral changes of CdSe/ZnS QD films from 30 to 200 °C.[36] (b) PL lifetime measurements of CDs. The leftmost plot shows time-resolved PL emission maps at 2, 50, and 80 °C (left to right). The rightmost plot presents PL lifetimes as a function of temperature.[38] (c) The top is an energy level diagram of Er^{3+} and Yb^{3+} illustrating upconversion luminescence mechanisms and the $^2H_{11/2} \rightarrow {}^4I_{15/2}$ and $^4S_{3/2} \rightarrow {}^4I_{15/2}$ transitions (green) used in FIR.The bottom shows the PL spectral changes of Er^{3+} from 25 to 300 °C.[39]

tion. The relative populations of these excited energy levels maintains a Boltzmann distribution and FIR of the resultant emissions enable self-referencing temperature sensitivity. For instance, Er^{3+} is widely used as a temperature probe often via green emissions from the TCLs $^2H_{11/2}$ and $^4S_{3/2}$.[39,49–59] These energy levels are populated via electron excitation to a higher energy level with subsequent non-radiative relaxation. With the low energy gap between $^2H_{11/2}$ and $^4S_{3/2}$, the $^2H_{11/2}$ state can also be thermally populated from the $^4S_{3/2}$ state. This population and depopulation process gives rise to relative variation in luminescence intensity between the TCLs. Analogous behaviors in Tm^{3+} ions,[60,61] Nd^{3+} ions,[52,62] and several others[63,64] have also been reported.

In upconversion of Ln^{3+}-doped nanostructures, low QY limits temperature sensitivity. As a remedy, many groups have sought to enhance Ln^{3+} luminescent efficiency by co-doping with sensitizers or altering the particle architecture. For instance, Tian et al. maximized luminescent intensity of Yb^{3+}/Er^{3+} co-doped $YNbO_4$ nanoparticles by systematically studying the effect of Yb^{3+} ion concentration on thermal sensitivity.[49] Here, Yb^{3+} served as a sensitizer, transferring energy to Er^{3+} to ultimately enhance FIR-relevant emissions. The authors successfully reported optimized temperature-dependent emission spectra over 25 to 400 °C. Other groups have altered nanocrystal size or structure to improve Er^{3+} luminescent efficiency.[52,65] Chen et al. introduced Yb^{3+}/Er^{3+} ions into a $NaGdF_4$-$NaYF_4$ core-shell host.[50] The group demonstrated an enhancement in Er^{3+} upconversion luminescence with increased $NaYF_4$ shell thickness. Here, the core-shell architecture shelters the luminescent Er^{3+} ions from non-radiative deactivation brought about by defects at the core surface. Tian et al. adjusted particle diameter of Yb^{3+}/Er^{3+} co-doped spherical Gd_2O_3 phosphors and found that temperature sensitivity increased with decreasing particle size, attributed to the more disordered local asymmetry environment in smaller particles.[54] While some of the investigated temperature ranges for Ln^{3+}-doped nanostructures are attractive for sensing in high-temperature polymer matrices (up to 1300 °C), in most of these studies, the nanocrystal host was dried to a powder form to ultimately serve as the matrix material. In a few instances, the nanocrystals were embedded in a glass ceramic medium.[39,58,59] It would be interesting to see these systems incorporated into a structural polymeric nanocomposite.

In addition to Ln^{3+}-doped materials, many organic fluorescent molecules are also employed for ratiometric sensing. Most common are fluorescent dyes that can impart temperature-sensing capabilities to polymer nanoparticles. For instance, Arai et al. designed nanoparticle thermosensors by embedding fluorescent dyes in poly(styrene-co-methacrylic acid) nanoparticles encapsulated by polyvinyl alcohol.[66] Temperature monitoring was achieved over 26-46 °C through the fluorescence ratio between a highly temperature-sensitive europium dye and an iridium dye with general temperature stability. Energy transfer within the

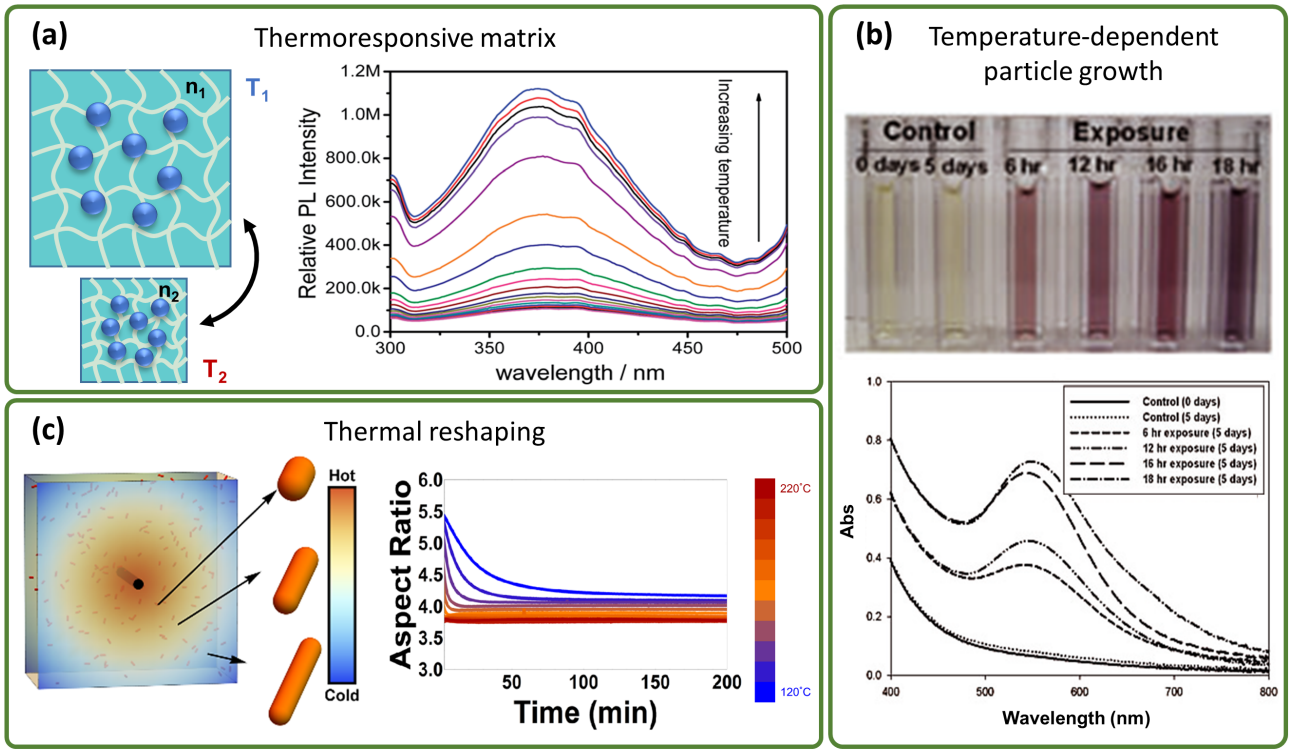

Fig. 5 (a) Schematic illustration of temperature-induced shrinking and swelling of poly(NIPAM-AAm) with embedded CDs (left). PL spectra of the hybrid nanogel over 16 to 50 °C at 280 nm (right).[42] (b) UV-vis absorption spectra of gelatin-templated AuNPs after exposure to 30 °C for durations ranging from 6 hr to 18 hr. Image depicts material color change with exposure time.[43] (c) Schematic illustration of AuNR thermal shape transformation when embedded in a structural composite (left).[44] AuNR aspect ratio as a function of time during isothermal holds from 120 to 220 °C (right).[45]

europium complex becomes increasingly non-radiative with increased temperatures, greatly reducing the fluorescence intensity at 615 nm. Driven by biological motives, the authors used this polymer-dye nanoparticle system to successfully map the internal temperature distribution within orally dosed endothermic fruit fly larva. Instead of employing two independent fluorophores, Ye et al. designed a moderately coupled ratiometric system with Rhodamine B (RhB) dye and semiconducting polymer dots.[67] Photoexcitation of the polymer was accompanied by fluorescence resonance energy transfer to the coupled RhB dye. Emission from the polymer dot served as an internal reference and temperatures from 10 to 70 °C were determined from thermal quenching of RhB luminescence.

Rather than relying on temperature sensitivity of molecules or isolated nanoparticles, extended nanostructures can also be used to measure the environmental temperature. One instance is exemplified in Fig. 5a. Wang et al. enhanced the temperature-dependent photoluminescence intensities of carbon dots by incorporating them into a thermoresponsive polymer matrix to produce a hybrid nanogel.[42] The matrix polymer experienced fully reversible, temperature-induced shrinking and swelling that manipulated fluorescence intensity through change in the surrounding refractive index ($n_1 \rightarrow n_2$). Fluctuations in the embedded CD fluorescence intensity were fully reversible and monitored environmental temperature changes over 16 to 50 °C.

Another highly investigated strategy for nanoscale optical sensing capitalizes on the plasmonic response of heavy-metal nanoparticles, namely colloidal gold. Gold nanoparticles (AuNPs) absorb and scatter light with incredible efficiency in a manner dependent on size, shape, and surrounding refractive index.[44,45] Surface plasmon (SP) resonances at visible and near-infrared wavelengths impart temperature sensing capabilities to AuNPs. As shown in Fig. 5b, both time and temperature during synthesis greatly impact AuNP growth and resultant particle size is reflected in the optical response. With this knowledge, Lim et al. sought to develop a AuNP system to monitor frozen food storage.[43] The authors designed a nano time-temperature indicator by correlating color signals from gelatin-templated AuNPs with temperature and duration of exposure. Here, gelatin served as both a reductant in the AuNP synthesis and as a stabilizing matrix. When the system was frozen at typical food storage temperatures (i.e. -20 °C), nucleation and growth of AuNPs halted. With stability in particle size, the system's optical response remained constant. Increased temperatures advanced nanoparticle growth in a time-dependent manner and consequently increased the optical density and shifted the plasmon wavelength. Similar thermal spectroscopic trends have been noted for ultrathin AuNP assemblies dried on quartz substrates.[68] Rather than relying on morphological changes of individual particles, thermal dewetting of AuNP films drastically modifies the shape of large-scale nanopar-

ticle assemblies and therefore affects the SP absorption band. With thermal treatment from 100 to 700 °C, a steady blue shift in SP absorption was observed and the band narrowed. Such spectroscopic shifts are consonant with morphological changes from large island assemblies to isotropic nanoparticles, suggesting that the average separation between AuNP islands increases and nanoparticle coupling decreases at higher temperatures.

Groups have surveyed the temperature sensitivity of colloidal gold by exploiting the anisotropic structure and thermodynamic instability of gold nanorods (AuNRs). Electronic charge oscillations in both the transverse and longitudinal directions of AuNRs give rise to two distinct, geometry-dependent localized surface plasmon modes. When thermally activated, AuNRs undergo shape transformation from elongated rods to more energetically favorable spheres as seen in Fig. 5c. The geometry-dependent optical response monitors the thermally driven particle shape change and serves as a platform for temperature sensing. Kennedy et al. applied this mechanism to map the thermal exposure of AuNRs embedded in a rigid epoxy matrix.[44] As a calibrant, nanocomposites were subjected to isothermal holds at various temperatures and the final, stabilized AuNR aspect ratio was computed from an analytical approximation for the Mie-Gans scattering theory. The authors found a linear dependence of the final aspect ratio on maximum exposure temperature over 100 to 200 °C. In a subsequent publication, this group explored the dynamics of AuNR shape transformation as influenced by particle size, geometry, and surrounding environment.[45] Their results illustrated the potential of tailoring AuNR systems for sensing in structural, high-temperature environments. For instance, the rate of AuNR shape transformation can be slowed by changing the polymer matrix rigidity around the nanorod, hindering atomic surface diffusion.[45,69] More dramatically, thermal reshaping can be suspended until temperatures as high as 700 °C by coating the particles in a thick (80nm) silica shell[70] or as high as 800 °C through yttria stabilized zirconia coating.[71]

Maity et al. also exploited AuNR anisotropy for local temperature sensing of aligned particles embedded in a polyethylene oxide matrix.[72] When exposed to ultrafast laser pulses of the same frequency of AuNRs' localized SP resonance, particles generated and dissipated heat into the surrounding matrix and locally melted the polymer. Matrix temperature in the immediate proximity of the nanorods was gleaned from measurement of particle rotation as demonstrated in the system's linearly-polarized extinction spectrum. Localized temperatures were sensed up to 95 °C.

As previously noted, the bulk of research in fluorescent and plasmonic nanothermometry is conceptualized and implemented with biological applications in mind. As a result, the analyzed temperature ranges and matrix materials are not suitable for the high-temperature (>300 °C) structural composites utilized in most material processing applications. However, the groundwork for developing optical nanosensors for structural polymers has been established, and many of the existing systems, particularly La^{3+}-doped nanocrystals and coated metallic nanoparticles, may already be stable under the necessary (high temperature, mechanically rigid) conditions. In the pursuit of next-generation temperature sensors, one must consider that both fluorescent and plasmonic strategies are sensitive to structural and dielectric changes in the nanoparticle environment. Great care must therefore be taken when working with temperature-responsive matrices or when comparing the same nanoparticle probe in different media.

5 Nanosensors of local viscosity

The ability to directly measure the viscosity of a liquid or gel can provide important insights into the mechanical response of the material, as well as for any chemical reaction mechanisms and kinetics that may be present. For example, the transport of biochemical reagents in both intra- and inter-cellular regions is influenced by spatial variations in viscosity of up to thousands of centiPoise per micron[73,74] and this has driven widespread interest in reliable, local measurements of viscosity in biological environments. The development of optical tools for measuring local viscosity has greatly benefited and influenced the cellular biology community in recent years.

The ability to directly measure viscosity with micron spatial resolution can also greatly enhance our understanding of mechanical and chemical processes in polymers and polymer matrix composites. The viscosity of a polymer melt can change several orders of magnitude as a result of the thermal history imposed by the manufacturing process. At the nanometer scale, viscosity affects the rate of crosslinking reactions during the cure of thermosetting materials. At the millimeter/centimeter scale, viscosity determines the flow of material inside a mold or autoclave. Bulk viscosity of polymers as a function of temperature is typically determined using viscometers or rheometers, but these methods are slow and are not always capable of reproducing the temperatures and pressures in the manufacturing environment. Furthermore, they require a minimum volume of material (commonly on the order of milliliters), and are therefore incapable of being applied with high spatial resolution. Our goal in this section is to highlight the recent key advances in the field of optical viscosity sensing, many of which apply directly to biological materials, and to identify the key advancements that are still needed in order for these techniques to have broader applicability in structural polymers.

The most widespread approach to optical viscosity sensing is, generally speaking, to take advantage of the influence of intramolecular motion on the fluorescence efficiencies and lifetimes in specifically designed fluorophores. Fig. 6 shows the general architecture along with several example molecular systems as discussed below. Each of the example molecules shown in Fig. 6 consists of at least two relatively rigid segments connected by one or more flexible bonds that allow the segments to bend, rotate, or otherwise move with respect to each other. The relative motions of the rigid segments changes the resonant electron or energy transfer between them, which can change the fluorescent properties of the molecule. This basic design principle has been shown to be effective for designing sensors suitable for sensing viscosity between 1-10000 cPs, with various advantages and disadvantages as discussed below.

For well over a decade, a common optical technique for measuring viscosity has been based on fluorescent molecular rotors (FMR). These molecules share a general structural feature that

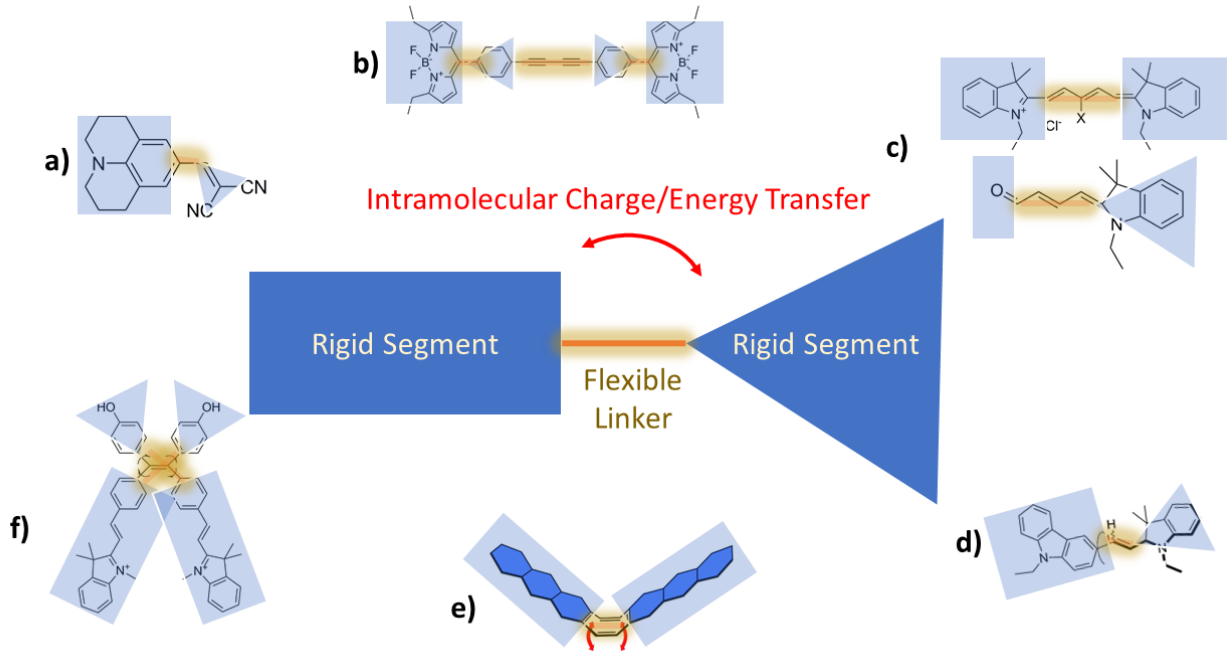

Fig. 6 Optical nanosensors for viscosity sensing comprise molecular species with rigid segments connected by a flexible linker. The linker can be rotationally free as in the case of (a)-(d) or may involve other degrees of freedom as in (e) and (f). Example molecules are from (a) 9-dicyanovinyljulolidine, Allen (2005)[75], (b) BODIPY homodimer, Raut (2014)[76], (c) RY3 and RY5 in Peng (2011)[77], (d) Donor-π-Acceptor compound comprising of benzo[b]thiophen-3(2H)-one 1,1-dioxide (BTD) as acceptor with carbazole moiety donor, Bhagwat (2018)[78], (e) FLAP molecule scheme from Kotani (2017)[79], and (f) tetraphenylethene (TPE), Chen (2018)[80].

allows for the rotation of one part of the molecule with respect to the rest, and an associated electronic structure known as a twisted intramolecular charge-transfer complex (TICT). In FMRs, the rotation is a non-radiative energy dissipation mechanism. When rotation is dampened, due to mechanical interactions in a viscous environment, the non-radiative pathway is suppressed and the associated fluorescent lifetime and intensity are increased. The basic mechanism was described in reviews by Haidekker and Theodorakis,[81,82] two of the pioneers and pre-eminent leaders in this family of materials. The approach has been exploited in a number of ways, and we highlight here some of the recent developments that have extended this basic molecular architecture.

The use of molecular rotors as local viscosity probes has found widespread use in the biomedical sciences, specifically in mapping the viscosity in intercellular and intracellular environments. Kuimova, et al. demonstrated viscosity sensing in live cells using the fluorescence lifetime of meso-substituted 4,4'-difluoro-4-bora-3a,4a-diaza-s-indacene. The response of this rotor to changes in local viscosity was demonstrated up to 960 cPs (see Fig. 7b).[83] The fluorescence lifetimes of their molecules are greater than 100 ps for all viscosities in that range, which makes viscosity determination by lifetime measurements accessible to common time correlated single photon counting detection schemes. Levitt et al. extended this approach by using two different meso-substituted boron-dipyrrin (BODIPY) molecules.[84] These were specifically designed to incorporate hydrophobic groups to make them soluble in cellular membranes, increasing the variety of biological environments whose viscosity can be imaged in this way. Raut et al. improved the ease with which BODIPY-based sensors could be synthesized and used by demonstrating the viscosity sensing of a homodimeric BODIPY up to $\sim$1500 cPs.[76]

A marked improvement in accuracy and reliability of molecular rotor viscosity sensing was achieved by combining molecular components to acheive ratiometric sensing. Haidekker, et al. showed ratiometric sensing using viscosity insensitive flourophores coupled to FMRs.[85] Further advances were made by Peng, et al. who synthesized a pentamethine cyanine dye meso-substituted with an aldehyde group (see Fig. 7c).[77] Their key achievement was to engineer simultaneous (dual-mode) ratiometric and fluorescence lifetime viscosity sensing into a single system. This approach was extended by Yang, et al. who demonstrated a fully self-calibrating dual-mode viscosity sensor in the form of a coumarin and boron-dipyrromethane (BODIPY) structure with a fixed spacing between the rotational elements (see Fig. 7a).[86] They attached their molecular sensors directly to mitochondria in order to map specific intracellular regions.

Recently, Chambers et al. also focused on organelle selectivity using the BODIPY based sensors.[87] Their approach achieves a large dynamic range (1-7000 cPs), temperature independence, fast response, and exquisite organelle specificity via targeted genetic probes. These characteristics, along with recent developments in microscopy, enable high resolution organelle viscosity imaging (ROVI). They showed that the ability to image viscosity at the microscale greatly enhances scientific understanding of

microscopic chemical processes in cells.

Important fundamental insights into the molecular mechanics associated with FMRs were recently provided by Ghosh, et al.[88] They used molecules with dimethylaniline and benzimidazolium groups (DABI) to systematically investigate the dependence of TICT sensitivity to the molecular ground state. Using synthetic, analytic, and computational techniques, they showed that viscosity sensing correlates strongly with the twisting relaxation rates, which depend on the ground state conformations. Similarly, Zhou et al. demonstrated the dependence of charge transfer efficiency on the conjugation of the flexible linker for a large number of molecular rotors.[89] They showed that there is no direct connection between the sensitivity to viscosity and the dipole moment of the rotors themselves, but rather that the charge transfer dipole dominates the sensing mechanism as well as the sensitivity to the polarity of the solvent.

More recently, the photoinduced electron transfer (PET) mechanism central to dual-mode molecular rotor sensors was extended to other types of conformational transitions in order to further expand the ability of these sensors to map viscosity across different intracellular organelles. Liu, et al. used molecules with both anthracene and 1,8-naphthalimide moieties to simultaneously exploit the dependence of PET and Forster resonance energy transfer (FRET) in order to improve the sensitivity to viscosity.[90] However, they focused only on environments with viscosities in the range of 60-945 cPs.

A variation on the intramolecular motion theme was recently introduced by Kotani et al. Instead of using FMRs they designed a “flapping” molecule having rigid aromatic wings and a flexible cyclooctatetraene joint(see Fig. 7e).[79] The flexible and aromatic photofunctional system (FLAP) changes between an angled (V-like) and flat (coplanar) configuration. This design minimizes the sensitivity of the fluorescence to the polarity of the surrounding solvent. As such, an important advantage of this solvent independence is the ability to measure viscosity in materials where the polarity changes along with the viscosity. The authors demonstrated this by monitoring changes in viscosity of an epoxy resin during cure. This is an important demonstration of the applicability of these molecular viscosity sensors to non-biological material systems.

Another phenomenon that has been used for viscosity sensing is aggregation-induced emission (AIE). In AIE the common phenomenon of concentration quenching of fluorescence is reversed; fluorophores that fluoresce weakly in good solvents are observed to increase their quantum yield significantly in poor solvents. As with FMRs, the increase in fluorescence upon aggregation is primarily due to the inhibition of molecular motions that provide non-radiative relaxation pathways. An excellent general description of this phenomenon, and a review of its broad applicability, has been published by Mei, et al.[92]

An early demonstration of the sensitivity of AIE dyes to high resolution viscosity sensing was made by S. Chen et al. using TPE-Cy, a hemicyanine dye[93]. They showed spatial mapping of the fluorescence lifetime in both intra- and intercellular regions, and they proved that the viscosity sensitivity could be decoupled from the aggregation resulting from mutual hydrophobicity in certain regions of the cell.

Recently, another AIE system was used by W. Chen, et al. to measure local viscosity during in vitro processes in which the intracellular viscosity changed dramatically.[80] Their work employed modified tetraphenylethene (TPE), adapted with hydroxyl groups to enhance solubility in water and with various cationic or proton receptor moieties for organelle specific targeting (see Fig. 7f).

A great deal of activity in the last few years has resulted in new molecules specifically engineered for compatibility in different environments or optical transitions at different frequencies. This has been enabled by excellent fundamental work in elucidating the underlying mechanisms of TICT and PET based viscosity sensing. For example, Avhad et al. developed coumarin morpholine-thiazole hybrid styryl dyes with greatly enhanced brightness and sensitivity to viscosity owing to their very large charge transfer dipole moments.[100] Similarly, Bhagwat et al. showed enhanced charge transfer dipoles, and associated nonlinear optical properties, of a family of thiophene/dioxide molecules (see Fig. 7d).[78]

In summary, the vast majority of work devoted to synthesizing and characterizing optically active molecular architectures for viscosity sensing have found inspiration and application in the biological sciences. For more specific insights, we refer the interested reader to an excellent review of fluorescence based sensing in biological materials by Zhu et al.[101] Fortunately, the activity in this field has provided the insights necessary to expand high resolution, optical viscosity sensing to a host of other material systems. In order to effectively apply these tools to structural materials such as polymers and polymer matrix composites two key advances are needed. First, molecules must be designed with a viscosity dependence that is inherently robust to changes in the polarity and temperature of the environment. It is unlikely that TICT based FMRs will ever meet this challenge, but the moderate success of the FLAP approach indicates that a rational design approach may yet succeed. Second, the range of viscosities to which these molecules are sensitive must be extended. The range of viscosities to which molecular sensors have been applied over the past decade is typically between .1-10000 cPs. In order to be useful in monitoring the process conditions of high-performance polymeric materials this must be increased by at least an order of magnitude.

6 Nanosensors of local stress/strain

In addition to chemical, temperature, and viscosity sensing, modulation in plasmonic, fluorescence, and phosphorescence signatures that arise from a variety of nano-constituents (quantum dots, nanoparticles, nanorods, molecular chromophores, etc.) in composite materials have been successfully used to measure and map local as well as global strain and stress.

The traditional method for optical stress and strain mapping involves DIC, or digital image correlation. In this technique, optical images of a material are taken before and after mechanical deformation, and the displacement of reference points in the material are tracked. While this method can provide information related to the deformation mechanism, residual stress, and other mechanical properties of the material of interest, the accuracy of

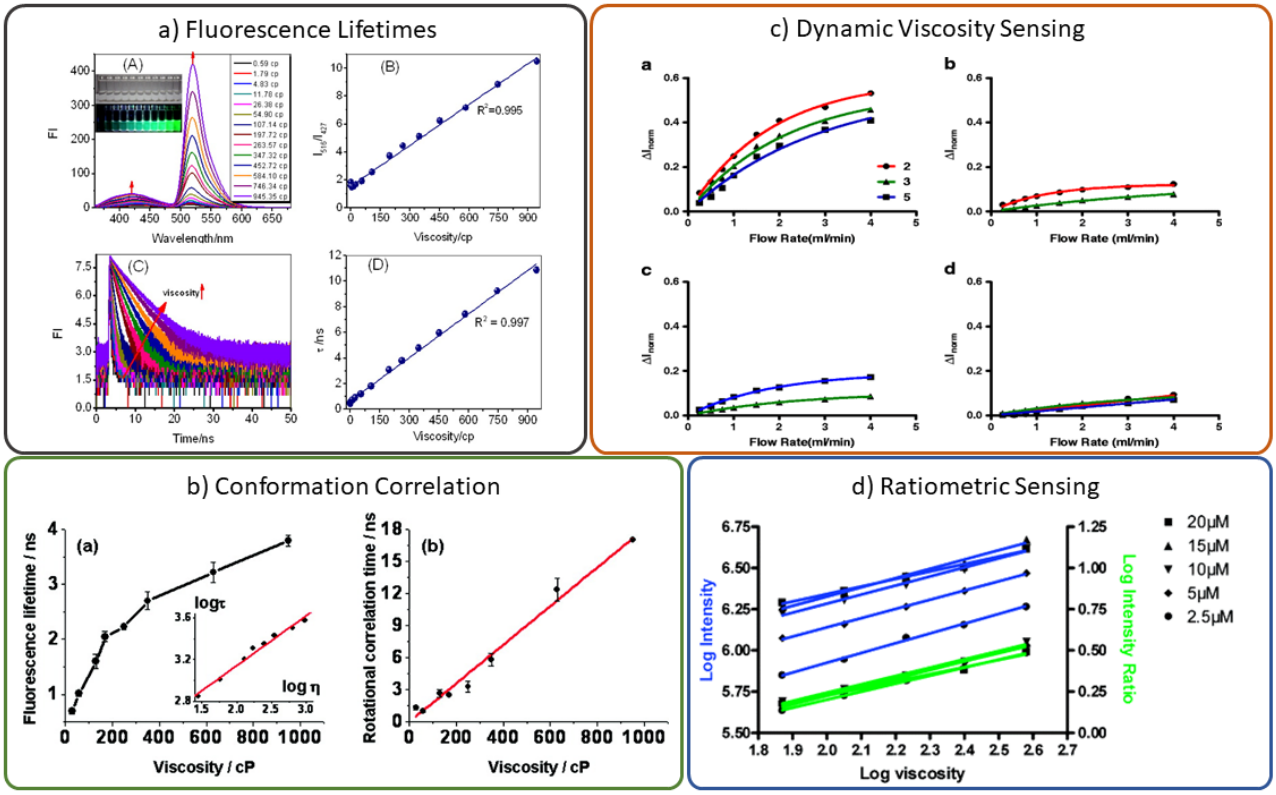

Fig. 7 Key advances in nanoscale molecular fluorophore viscometry include (a) quantification of the fundamental fluorescence lifetime changes in FMRs[86], (b) establishment of the relationship between molecular conformation and viscosity sensing[83], (c) demonstration of dynamic viscosity sensing[91], and (d) development of ratiometric (self-calibrating) viscosity sensors[85].

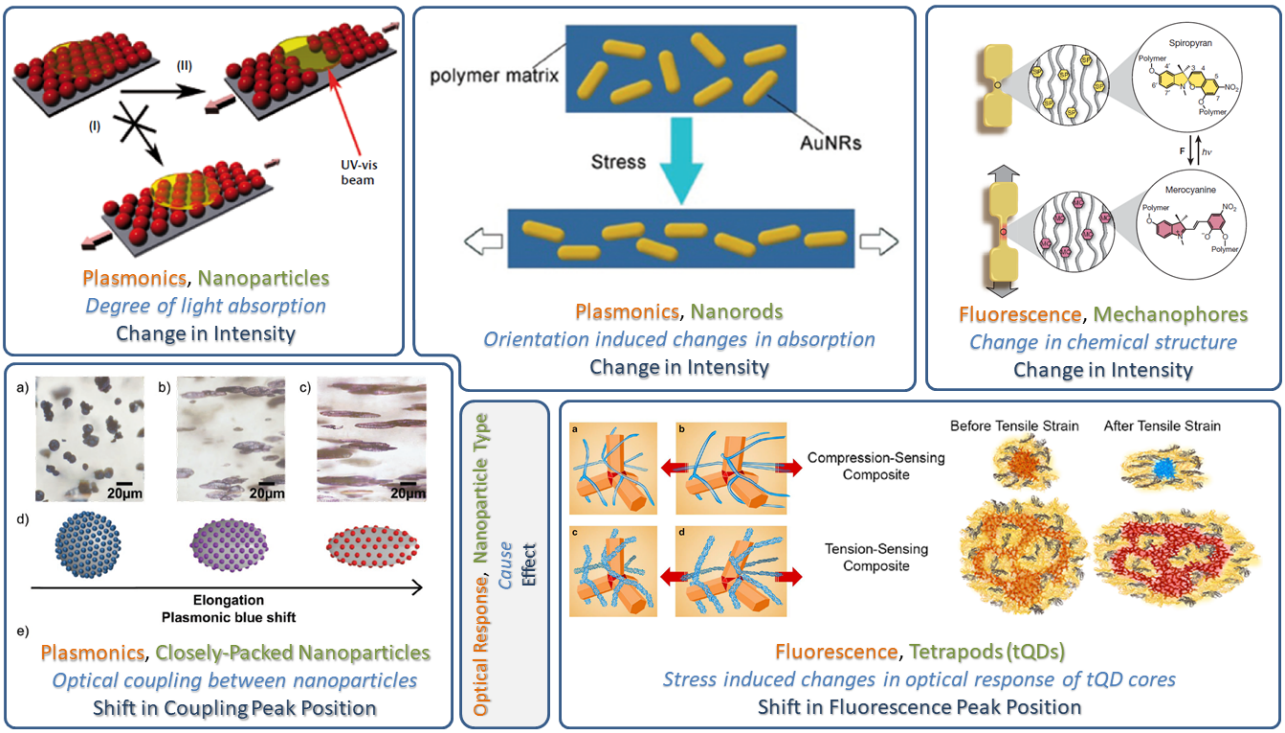

Fig. 8 Schematic representation of different approaches which are undertaken to map stress/strain in composite materials using plasmonic and photoluminescence routes. The text-colors can be read as follows: orange: type of optical mechanism; green: nanoparticle type; light blue: physical changes in the structure that causes modulation of optical response; dark-blue: optical characteristic whose modulation is read out. The schematic images are taken from Refs[94](Top-left), [95](Top-center), [96](Top-right), [97](Bottom-left), and [98,99](Bottom-right)

the data is strongly reliant on the imaging system and only the surface of a material can be probed.[102,103]

Molecular stress/strain sensors offer an alternative approach to DIC that can be implemented with relative ease. Furthermore changes in optical signatures to sense mechanical response provides a non-invasive approach, and thus, have a huge potential not only in biological applications where non-invasiveness is a key requirement, but also in a number of aerospace applications where estimating *in-situ* mechanical response (such as residual strain/stress and crack initiation or growth) under applied load or physical aging is critically important. In Fig. 8, we schematically highlight a few key nano-constituent design frameworks (such as nano-constituent types as well as their arrangement) which have been explored to date towards sensing either stress or strain in composite materials. Below, we have outlined and categorized the research progress to date in terms of different types of nanoparticle and molecular entities for stress/strain sensing, specifically in organic matrices, via different types of optical responses.

Due to their intrinsic inert nature, Au nanoparticles (AuNPs) have been widely explored in both research as well as commercial applications in a number of applications, and as a consequence also found their applicability as stress/strain sensors in composite materials. For example, Ryu and co-workers employed the Poisson's ratio framework to calibrate strain-sensing capability in PDMS-AuNP films.[104] Under strain, decrease in thickness reduced the overall absorbance of light around 530 nm, which was mapped back to degree of applied strain. Similarly, using $Au@SiO_2$ nanoparticles deposited on the PDMS films, Correa et al. demonstrated that changes in the absorbance of surface plasmon peaks of gold nanorods can be used as a measure of overall strain within the film (Fig 9a) as well as to detect early stages of structural damage.[94] The authors also reported that when AuNPs were deposited as an ordered array of holes over a PDMS film can, changes in the light diffraction upon stretching could provide an alternative means to measure applied strain.

Optical coupling between closely-packed nanoparticles has also been identified as one of the key plasmonic features towards identifying mechanical deformation in composite systems, where inter-particle distance change under deformation is reflected as shifts in coupling peak (blue-shift with increasing distance and vice versa). For example, Cataldi and co-workers demonstrated a method to trigger the coupling between Au nanoparticles embedded on the PDMS surface by mechanical strain as well as growing nanoparticles (once the growing sites were immobilized within the PDMS matrix).[105,106] The inter-particle distance was observed to decrease with growth time as well as along the perpendicular direction to stretch, which was manifested in increased inter-particle coupling as evident from red-shifts in the coupling peak. Similarly, Millyard et al. embedded 20 nm AuNPs in PDMS and reported strong blue-shifts (around ∼700 nm peak) under both uniaxial and bi-axial strain.[107] As depicted in Fig. 9b, the authors reported larger sensitivity for uniaxial strain when the light-polarization was parallel to strain direction. A similar blue-shift was also observed by Minati and co-workers for 10 and 60 nm AuNPs embedded in PDMS substrate.[108] Recently, Burel et al. infused AuNPs in spherical silica capsules (30-60 nm) in PVA matrix for strain detection.[97] Under stretching, the capsules elongated in shape, increasing the distance between the gold nanoparticles, which was reflected in observation of blue shifts in coupling plasmon peak. Interestingly, Bohm et al. also observed a similar effect in Au nanorods (AuNRs), where the authors embedded 2D gold nanorod arrays in epoxy films for strain detection and observed shifts of LSPR peaks (∼20 nm for 15% tensile strain).[109] The shift was attributed to the decrease in optical coupling due to increase in inter-rod distance.

Sannomiya et al. embedded 50 nm gold nanoparticles in PDMS and calibrated changes in the optical coupling between the nanoparticles as a strain-mapping feature.[110] They reported that due to inter-particle distance change under deformation, the coupling mode showed larger differences in extinction for perpendicularly polarized light (with respect to stretch direction), which was used as a measure of strain with the sample. Minnai and co-workers used supersonic cluster beam implantation to implant neutral Au clusters in PDMS up to 45 vol% and reported plasmonic shifts of 180 nm under stretching.[111] Under cyclic deformation, the authors observed different degree of reduction and even disappearance in peak shifts based on initial vol% and attributed it to rearrangement and reorganization of the embedded clusters during cycling. Recently, Marin and co-workers used the inter-particle distance modulation feature under strain towards developing a peizoplasmonic sensor with detection sensitivity of 0.002% strain via depositing nano-islands of gold and silver on graphene, functionalizing the gap between nano-islands via benzenethiolate and characterizing the SERS signal.[112] Under mechanical strain, the increased gap between nano-islands attenuated the electric field, which in turn drastically reduced the SERS signal.

In addition to inter-particle optical coupling, the physical and optical anisotropy of AuNRs (such as relative orientation of long axis with respect to applied strain) have also been exploited for sensing stress/strain in composites. Fu et al. exploited orientational dependence of LSPR peak in Au nanorods and developed a pressure-responsive film by incorporating AuNRs in PVA/PEG polymeric matrix.[95] It was reported that transverse:longitudinal peak intensity ratio depends upon the degree of orientational order of nanorods within the film. Upon stretching, the polymer deformation modified the nanorod orientation, which was reflected as modification in peak intensity ratio. The authors also suggested that a variety of knobs, i.e. intensity and duration of applied pressure, nanorod's aspect ratio, and fluidity of the matrix (relative ratio of PVA/PEG), can be employed to modulate the pressure sensitivity of the films (via relative ratio of TSPR and LSPR peak intensity as shown in Fig. 9c). In a later study, the authors demonstrated the similar effect by incorporating Ag@Au triangular nanoplates (NPL) along with Au nanoparticles in polyvinulpyrrolidone (PVP) composite films.[116] In a different approach, Orendroff et al. estimated local deformation under uniaxial loading with a large aspect ratio (∼16) AuNR-PVA system via applying digital image correction techniques on resonant Rayleigh scattering data, where authors reported that the light pattern maintained its integrity over relatively large deformation.[117]

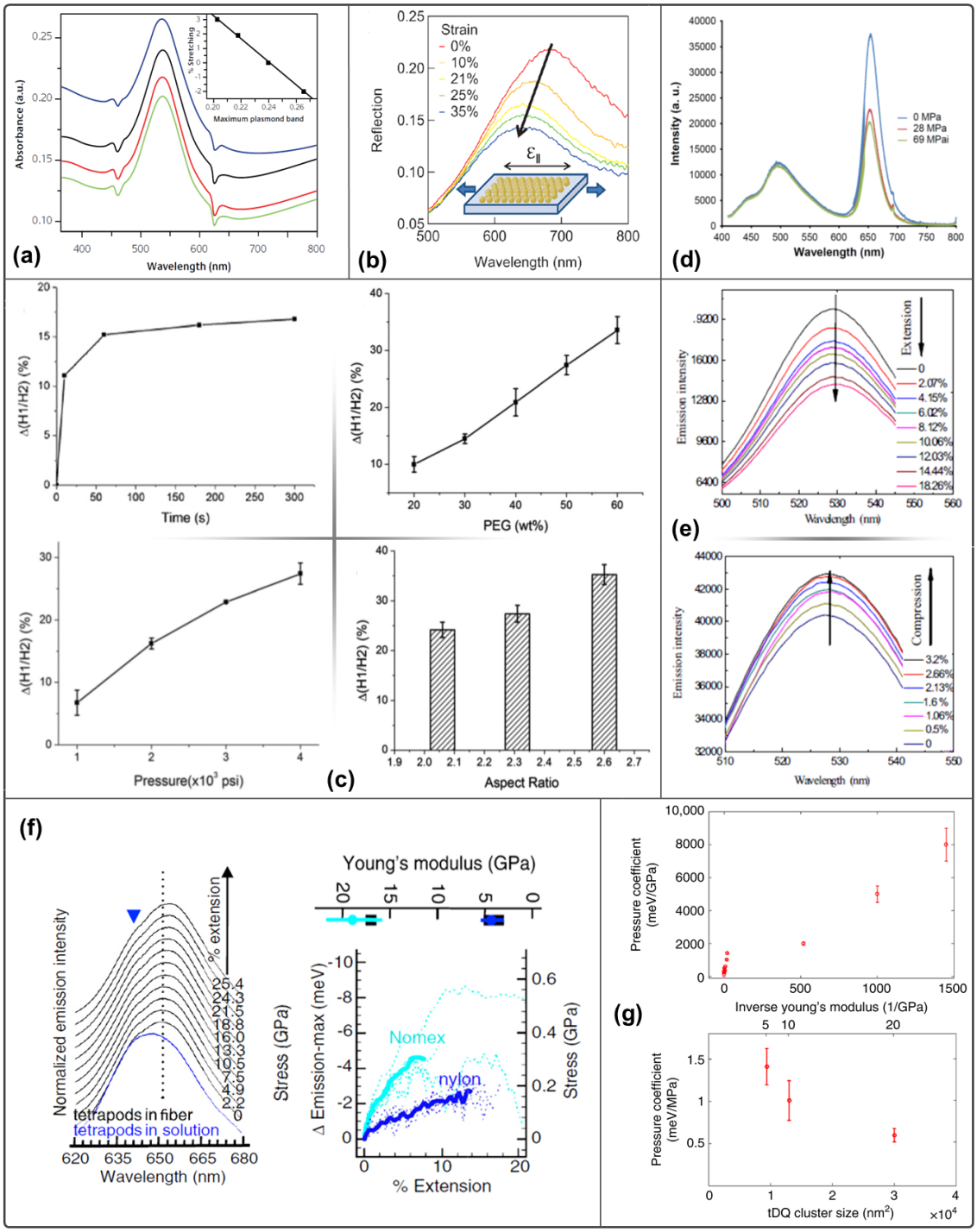

Fig. 9 (a) UV-vis spectra of an Au@SiO2 nanoparticle deposited onto PDMS film.[94] Spectra correspond to as-prepared (black), 2% stretch (red), 3% stretch (green), 2% compression (blue). Inset shows the linear dependence as a function of tensile and compressive stretch; (b) Reflection spectra of Au-nanoparticle mats under uniaxial increasing strain parallel to optical polarization;[107] (c) Plot of Δ(H1/H2), i.e., relative change in intensity ratio, for the film experiencing a fixed pressure for different times (top-right), different pressures (bottom-right), different fluidity of matrix in terms of changes in PEG concentration (top-left), and aspect ratio (bottom-left);[95] (d) Changes in QD fluorescence intensity (right peak) with increasing pressure in 9 nm QD nano-composite cube as compared to the epoxy fluorescence (left peak) which is stable with pressure;[113] (e) Tensile (top) and compression (bottom) test spectra of QDs-epoxy resin nano-composite system, showing decrease (increase) in photoluminescence intensity as a function of tensile (compressive) strain;[114] (f) (Right) Fluorescence spectra of tQDs embedded in a single polyester fiber under extension where a fluorescence red shift is clearly observed with increasing strain.[115] A spectral shoulder is also shown to match the tQDs in solution (blue arrow). (Left) Emission maxima of tetrapods in Nomex® (cyan) and nylon (blue) single fibers as a function of fiber extension (dotted lines) and the corresponding average (solid lines) demonstrating an accurate measure of the Young's modulus of these fibers (black data points on the scale-bar are taken from literature. The error bars represent the error in calculated modulus due to linear fit); (g) (Top) Monotonic scaling of the tQD pressure coefficient (measure of sensitivity) over three orders of magnitude with the polymer inverse Young's modulus.[99] (Bottom) Plot of the pressure coefficient as a function of tQD cluster size for three concentrations of tQDs in poly(styrene-ethylene-butylene-styrene). Error bars represent standard error of the mean (SEM), where each mean is the average of 10-15 measurements.

While gold based nanoparticles have been the 'popular' choice among nanoparticles due to their distinctive chemical and physical properties, ease of synthesis, functionalization, inertness to biologically environments, and high absorption cross-section at visible and near-infrared wavelengths, several other nanoparticle chemistries as well as geometries have also been explored to measure and map local/global strain and/or stress response in composite materials. For example, as shown in Fig. 9d, Ford et al. demonstrated pressure-sensitive epoxy nanocomposites with spherical CdSe/ZnS core-shell quantum dots (QDs) which could detect pressure changes in MPa range via monitoring the normalized fluorescence intensity.[113] The authors reported a 20% change in the intensity under applied load of 60 MPa for ∼9 nm QDs. Interestingly, the response was only observed for 9 nm nanoparticles (largest studied in the study) and was speculated to be caused by "constraint of specific sites on the QD exterior caused by stress translated through the ligands, affecting coupling between surface states." Later, Yin and co-workers investigated photoluminescence response in smaller QDs (2-5 nm) in epoxy matrices and observed the 30% decrease in intensity under 18% tensile strain along with 6% increase in 3.7% compressive strain (see Fig. 9e).[114] Unlike Ford and co-workers, Jia et al. observed a non-monotonic response in fluorescence intensity under strain for CdSe@CdS QDs capped with amphiphilic block polyarylene ether nitrile (amPEN) in PDMS matrix.[118] Here, the initial enhancement (until 50% strain) was attributed to the stretch-induced dilution of doped QD/amPEN fluorophores, which effectively relieved the fluorescence quenching of highly concentrated QD/amPEN superparticles. The subsequent reduction in fluorescence intensity was possibly attributed to the dilution of fluorophores concentration in detected area due to stretching. In an different approach, Fischer et al. investigated the optoelectronic behavior of individual core/shell CdSe/CdS nanocrystals via applying compressive force (on individual nano-crystals) via atomic force microscopy and compressive stresses up to 3.8 GPa can be sensed via either red or blue-shifts (originated from nanocrystal orientation with respect to compressive force direction) in emission spectra.[119]

Tetrapod quantum dots (tQDs), a more exquisite nanoparticle geometry than spherical core-shell QDs (see Fig. 9), have also been continually explored for stress/strain sensing in composite materials via optical response. tQDs are nanocrystals consisting of a semiconducting core and four protruding arms. When embedded in the matrix, these arms are susceptible to nano-newton forces due to deformation of surrounding matrix and alter the optical response of the core under tensile or compressive perturbation[120]. Choi and coworkers observed red-shifts in the photoluminescence emission of CdSe-CdS (core-arm) tQDs embedded in polyester fiber under uniaxial strain as shown in Fig. 9f.[115] The authors suggested the tQDs possess better sensitivity than nanorods, where arm length of 25 nm were found to be optimal for highest stress-mapping sensitivity. In addition, the authors calibrated the stress-strain response via modulus comparison (with and without tQDs polyester) and subsequently estimated the Young's modulus of tetrapod-containing Nomex and Nylon fibers within 5% (Fig. 9f). Later, the author incorporated the tQDs within poly L-lactic acid (PLLA) fiber via electro-spinning process and confirmed that the inclusion of tQDs up to 20 wt% have minimal impact on intrinsic mechanical properties (such as modulus) of the fiber, also providing repeatable stress-sensing ability over multiple cycles with minimal hysteresis in peak shifts.[121] It was suggested that poor stress transfer to tetrapods during applied strain (possibly due to weak interface affects) prevented permanent deformation of the tetrapod and was reflected in the lack of hysteresis in emission spectra. In 2016, Raja et al. observed both red-shifts as well as blue-shifts (unlike previous studies) in the emission spectra and attributed it to the observation (based on simulation) that not only concentration, but the packing (morphological arrangement) of tQDs aggregates have significant impact on the direction of the shift (denser close-packing led to blue-shifts in compression-sensing films and vice versa).[98] The authors suggested that blue-shifts (red-shifts) are due to compression (tension) of the tQDs' core during the overall tensile deformation of the nanocomposite. Building upon their previous work, the authors recently functionalized tQDs with multiple functionalities and investigated 17 different tQDs-polymer systems (8 different polymers with Young's modulus varying over 4 orders of magnitude) along with different concentration and dispersion profiles.[99] Here, as demonstrated in Fig. 9g, the authors observed that changing the modulus of the host matrix has a notable effect on degree of tQD stress response (varying over 3 orders of magnitude) with higher sensitivity observed for compliant matrices. Moreover, the stress sensitivity was found to be higher with small tQDs clusters. The observed behavior (degree of sensitivity) was attributed to a number of possible factor including a) changes in the tQD dispersion; b) changes in the tQD interfacial chemistry with matrix; c) amplification of stress around the tQD-polymer interface chemistry; and d) varying degree of strain transfer from polymer to tQDs.

Zullfrank and co-workers employed a different materials chemistry and investigated ZnO tetrapods as stress sensors in PDMS matrix. Unlike the tQDs mentioned previously,[98,99,115,121] ZnO tetrapods didn't exhibit any difference in composition between arms and core. Under tensile strain at 15 wt% loading of ZnO tQD filler, the authors observed the decrease in ratio of the green emission and exciton emission ($A_{green}/A_{exciton}$) increasing tensile strain. The decrease in emission was hypothesized to occur from stress and the generation of defects sites on the ZnO tetrapods. While they did not directly measure the modulus, the authors concluded that the ZnO tetrapods' network could be used to calculate the tensile elasticity of other materials, simply from the Agreen/Aexciton ratio and an applied strain on a material.[122]

It is noted that while different types of discussed nanoparticles have been successfully used to measure, map and calibrate both global and local mechanical state of composites (stress/strain), there are only a handful of tQDs based studies for estimating intrinsic properties, such as tensile or compressive modulus.[98,99,115,121] These studies measure a 'bulk' value of modulus and have essentially relied on the observation that inclusion of tQDs do not noticeably alter the intrinsic modulus of the matrix, although it was suggested that the detection limit of the tetrapod was limited to the modulus of the tetrapod itself, i.e., a

tetrapod with a smaller modulus than the matrix will move with the matrix, preventing accurate elastic measurements.[115] The lack of sensors focusing specifically on the modulus of a system may stem from the realization of the target application (damage sensing, tissue material deformation, etc.) from stress or strain measurements alone and thus, provide an opportunity for sensing/measuring modulus at nano and micron scale. Furthermore, the modulus sensors would provide real-time damage feedback during the lifetime of a material or enable quality control analysis during manufacturing processes, not only for soft materials such as organic matrices, but also for stiffer, structural materials, all of which are essential in the aerospace industry.

As a material alternative to complex inorganic nanoparticles, a number of organic as well as hybrid (organic/inorganic) 'molecular' entities have also been successfully employed to optically sense stress/strain. Cellini et al. reported strain-sensing via correlating mechanical and optical (fluorescence emission) response of TPU-BBS (thermoplastic polyurethane, bis(benzoxazolyl)stilbene dye) blend.[123] While emission ratio, I_{436}/I_{493} (monomer (436 nm) of excimer emission (493 nm) ratio), did not directly correlate with the stress within the material, the authors observed a linear relationship between the degree of stretch within the polymer and I_{436}/I_{493} ratio as also can be seen in Fig. 10a. The variation in the ratio were attributed to reorganization of dye aggregates within the elastomeric network with respect to applied deformation. Under loading, a relative increase of the emission in the monomer band was observed while an increase of emission in the excimer band was observed during unloading. The authors also suggested that as TPU-BBS dyes have a low modulus, they could be useful for sensing small forces at high strains. In a follow-up study, the authors further confirmed the observed behavior for a number of dye concentrations as well as under bi-axial stretching.[123] Among studied dye concentrations (up to 1.5 wt%), TPU-BBS blends with 0.5 wt% resulted in highest variation in emission ratio (see Fig. 10a inset), suggesting that identifying an optimal value is crucial to enhance the sensitivity of the mechanochromic sensor device. Yeroslavsky and co-workers incorporated a pair of acceptor and donor dye (fluorescein and rhodamine B) into elastomeric PDMS films to evaluate strain sensitivity as well as local strain visualization.[126] Under tensile deformation, increased distance between donor and acceptor molecules lead to decrease in energy transfer efficiency, which in turn was manifested as relative increase (decrease) in emission from fluorescein (rhodamine B) dye.

Shou et al. synthesized a block-copolymer of Poly (ethylene terephthalateco-1, 4-cylclohexylenedimethylene terephthalate (PETG) - polyethelyne glycol (PEG) with varying PEG % up to 30% and suggested that the flexible PEG segment contributes to the fluorescence emission of the copolyester due to the formation of ultrasmall ($\sim$5 nm) luminescent carbon nanodots.[124] As seen from Fig. 10b (and inset), a monotonic repeatable decrease of fluorescence intensity was observed under stretching up to 130% which was attributed to the dilution of carbon nanodots (per unit surface area) upon stretching. Filonenko and co-workers incorporated phosphorescent copper complexes into main-chain polyurethane and developed a fully reversible mechanical stress phosphorescent sensor which didn't require any changes in molecular structure or rearrangement but only relied on the suppression of non-radiative relaxation under elevated stress.[127] The studied copper complexes were observed to be extremely sensitive to the changes of nearby surrounding environment and were reflected in increase in the relative intensity with increasing stress (as well as excitation power). The authors also demonstrated that such an approach can be used to easily monitor local stresses via direct optical imaging.

Mechanophores, or compounds that change chemical structure under external applied stimuli, represent another area of stress/strain sensors. Davis and coworkers showed that spiropyran, when covalently bound to a polymer, converts to merocyanine under applied stress to the polymer, leading to change in the green intensity as shown in Fig. 10c.[96] This mechanical induced activation was observed to happen along the C-O bond of the spiropyran. Furthermore, as merocyanine is also fluorescent, it can be used as a damage sensor and molecular probe. In a different study, Woodcock et al. used rhodamine spirolactam as a mechano-fluorescent probe to detect the strain on the interface of silk fibers.[125] Here, the activation of fluorescence was associated with the ring opening of the lactam under applied strain in presence of small amount of water (please refer to Fig. 10d for observed color change due to fluorescence). It is however unknown how both of these mechanisms work. It was posited that ring-opening mechanism either occurs through stress transfer to the covalent bonds of the lactam or frictional shear is responsible, similar to the findings of Davis and coworkers.[96] The authors used fluorescent lifetime imaging to observe the silk fibers after critical failure, and were able to map regions of lower and higher local stresses. Finally, they found that covalent immobilization rather than physisorption to the fiber was crucial, as it provided longer average and more narrow fluorescent lifetimes for fluorescent imaging.

Similar to plasmon based sensing via nanoparticles, a 'molecular' approach has only been demonstrated for soft-materials towards sensing mechanical response as evident from the discussion above. We believe that developing strategies to incorporate these molecules in stiffer matrices will be useful in a number of aerospace and other industrial applications from the perspective of non-invasive monitoring of structural damage over time. Moreover, as in plasmonics, while these approaches also provide a visual guide to locally identify regions with high stress or strain, currently there are no framework to estimate to microscopic/nanoscopic moduli of the materials of interest and hence, it is timely that such approaches be developed as well.

7 Discussion and Conclusion

Optical nanosensors for measuring local chemical species, temperature, viscosity, stress, and strain have been developed using both molecular and nanoparticle architectures, but their application in structural polymer matrix materials is limited by challenges in sensitivity and specificity of their response.These challenges can be overcome by combining sensing modalities into a unified nanosensor architecture that is either robust to extraneous environmental changes or inherently self-calibrating via a multi-

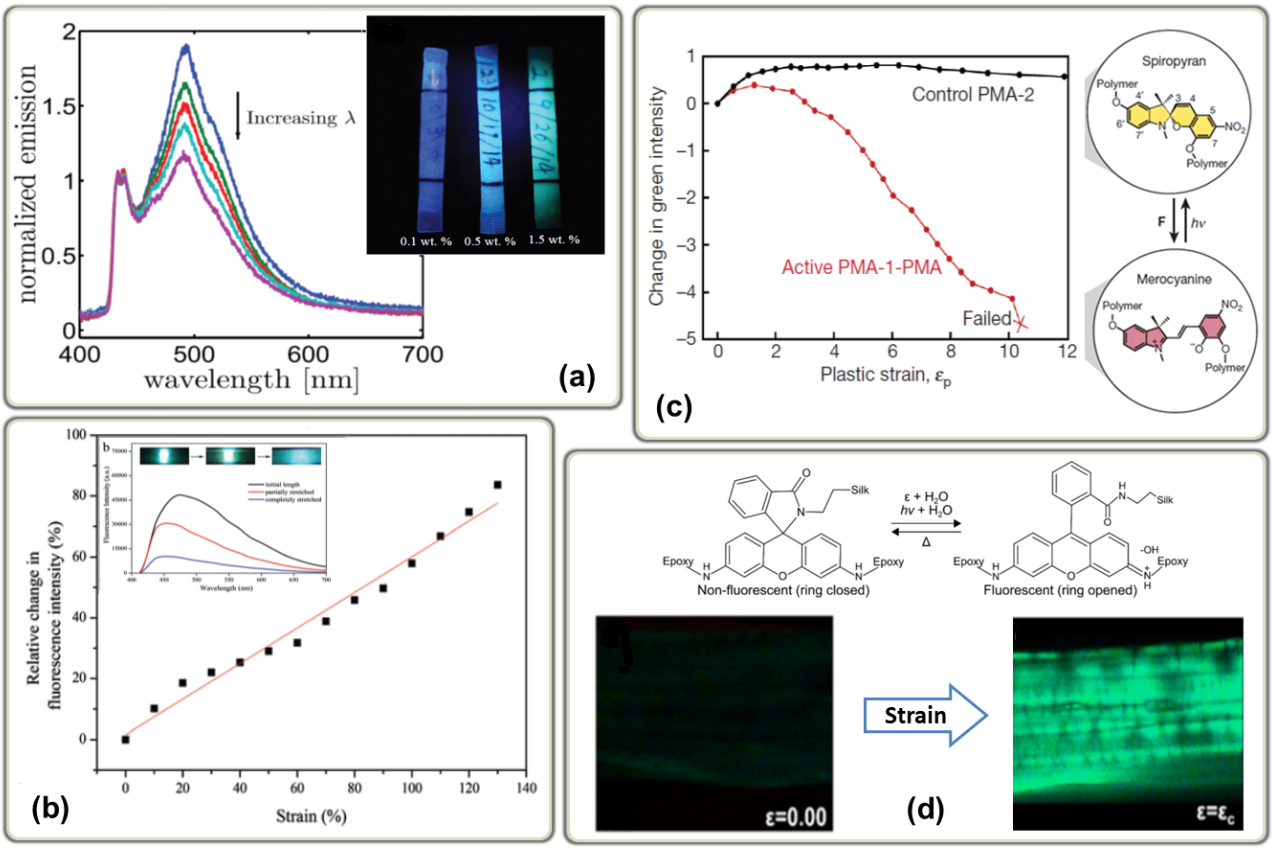

Fig. 10 (a) Normalized emission spectra of a TPU-BBS blend at 436nm as a function of the progressive stretch of the sample during the loading phase.[123] Blue (top) to purple (bottom) are spectra obtained for increasing stretch levels from blue, I=1.00 to I= 2.04. The inset shows the photoluminescence for 3 different dye concentrations (0.1%. 0.5% and 1.5%); (b) Fluorescence emission spectra of PETG-PEG co-polyester containing 10 wt% PEG at different stretching states.[124] The inset shows the linear fitted line of dots of relative change in fluorescence intensity; (c) Accumulation of plastic (unrecovered) strain and relative change in green intensity for active PMA-1-PMA and a PMA-2 control samples after each loading cycle in a fatigue test;[96] (d) (top) Proposed activation mechanism for the ring opening of the spirolactam through applied energy and in the presence of water; (bottom) Fluorescence images showing Significant activation of the mechanophore (Rhodamine 110) in response to uniaxial mechanical strain.[125]

modal response.

From the perspective of structural composite materials, the most technologically mature, robust, optical nanosensors are those that are responsive to temperature. Temperature sensors based on fluorescent or plasmonic nanoparticles are readily available that are compatible with structural polymers and that function over relevant temperature ranges. The primary challenge to the robustness of these sensors remains their specificity. In other words, the shifts in scattering or emission spectra of nanosensors embedded in a structural polymer are influenced by changes in local chemistry and pressure. In order for these nanosensors to achieve the necessary precision the community must develop new architectures that can account for these convoluted stimuli.

By contrast, the use of optical nanosensors for detecting changes in chemistry within a structural polymer (e.g., as a result of crosslinking reactions or degradation) is almost nonexistent. Given the degree to which nanoscale chemical sensors have been developed for detecting specific analytes in gas or liquid phases, there is an enormous opportunity to design nanomaterials to be responsive to changes in polymer chemistry in the solid phase. Because the spatial extent of their response is relatively large, plasmonic based sensors are particularly attractive for this purpose. However, existing techniques for making the plasmonic response chemically specific are unlikely to work in the solid phase. Thus, new strategies must be developed.

The sensing of mechanical properties, such as viscosity, stress, and strain, is uniquely challenging in structural polymers. Ideally, sensors are desired that can respond to changes in complex modulus over many orders of magnitude, and this is not likely to be acheived by a single nanosensor. Advances in nanoparticle based viscosity and strain sensing in recent years suggest that these challenges might be met by combining viscosity-dependent fluorophores with functional groups that couple directly to the polymer resin. To reiterate, the advantage of these sensors is that they provide local temperature, chemical, pressure, and/or viscosity information at relatively high resolutions using optical sensing. Rather than a bulk measurement of a given material parameter, these sensors are able to detect variations of the material parameters across the manufactured part which is incredibly relevant in assessing failure risk in a part as it is along these regions of high variation where failure is most likely to occur. A disadvantage of these sensors are the cross-correlations between the optical readout and variations of multiple material parameters, which we have heavily emphasized in this review as a problem

to be solved. Another disadvantage is the fact that these sensors must be implanted into the material during the manufacturing process and are not, as it were, reusable from part to part.

The potential impact of optical nanosensors for chemistry, temperature, viscosity, stress, and strain in structural polymer composite materials is high. The ability to quickly and precisely assess material properties that govern resin flow and cure can lead to significant cost reduction and improved performance of these increasingly important materials. While optical nanosensors have found widespread use in a variety of material systems, their use in structural polymers has been limited. In the coming years we expect that challenges in sensor robustness and specificity will be addressed by applying the foundational principles that have been developed in other fields to this challenge.

Conflicts of interest

There are no conflicts to declare.

Acknowledgements

The authors acknowledge the support of the Materials and Manufacturing Directorate of the Air Force Research Laboratory. This work was supported in part by the Air Force Office of Scientific Research (Program Officer: Dr. Byung-Lip "Les" Lee; Grant Number: 16RXCOR324).

Notes and references

1 R. Ma, Y. Wang, H. Qi, C. Shi, G. Wei, L. Xiao, Z. Huang, S. Liu, H. Yu, C. Teng *et al.*, *Composites Part B: Engineering*, 2019, **167**, 396–405.

2 Z. Guo, Y. Zhu, J. Chen, X. Cui, Q. Yu, M. Dong, J.-x. Zhang, J. Fan and C. Wang, *Journal of Materials Chemistry C*, 2019.

3 G. Zhu, X. Cui, Y. Zhang, S. Chen, M. Dong, H. Liu, Q. Shao, T. Ding, S. Wu and Z. Guo, *Polymer*, 2019, **172**, 415–422.

4 H. Liu, Q. Li, S. Zhang, R. Yin, X. Liu, Y. He, K. Dai, C. Shan, J. Guo, C. Liu *et al.*, *Journal of Materials Chemistry C*, 2018, **6**, 12121–12141.

5 C. Wang, V. Murugadoss, J. Kong, Z. He, X. Mai, Q. Shao, Y. Chen, L. Guo, C. Liu, S. Angaiah *et al.*, *Carbon*, 2018, **140**, 696–733.

6 Q. Chen, Q. Yin, A. Dong, Y. Gao, Y. Qian, D. Wang, M. Dong, Q. Shao, H. Liu, B.-H. Han *et al.*, *Polymer*, 2019, **169**, 255–262.

7 D. Jiang, V. Murugadoss, Y. Wang, J. Lin, T. Ding, Z. Wang, Q. Shao, C. Wang, H. Liu, N. Lu *et al.*, *Polymer Reviews*, 2019, **59**, 280–337.

8 P. Bosch, F. Catalina, T. Corrales and C. Peinado, *Chemistry – A European Journal*, 2005, **11**, 4314–4325.

9 S. A. Maier, M. L. Brongersma, P. G. Kik, S. Meltzer, A. a. G. Requicha and H. A. Atwater, *Advanced Materials*, 2001, **13**, 1501–1505.

10 L. Walekar, T. Dutta, P. Kumar, Y. S. Ok, S. Pawar, A. Deep and K.-H. Kim, *TrAC Trends in Analytical Chemistry*, 2017, **97**, 458–467.

11 N. Jiang, X. Zhuo and J. Wang, *Chemical Reviews*, 2018, **118**, 3054–3099.

12 J. Fleischer, R. Teti, G. Lanza, P. Mativenga, H.-C. Möhring and A. Caggiano, *CIRP Annals*, 2018, **67**, 603–626.

13 *Creep and Fatigue in Polymer Matrix Composites*, ed. R. M. Guedes, Woodhead Publishing, San Diego, 2nd edn., 2019.

14 H. Qi, M. Teng, M. Liu, S. Liu, J. Li, H. Yu, C. Teng, Z. Huang, H. Liu, Q. Shao *et al.*, *Journal of colloid and interface science*, 2019, **539**, 332–341.

15 L. Tang, S. Li, L. Xu, W. Ma, H. Kuang, L. Wang and C. Xu, *ACS applied materials & interfaces*, 2015, **7**, 12708–12712.

16 C. Hao, H. Kuang, L. Xu, L. Liu, W. Ma, L. Wang and C. Xu, *Journal of Materials Chemistry B*, 2013, **1**, 5539–5542.

17 W. Yan, L. Xu, W. Ma, L. Liu, L. Wang, H. Kuang and C. Xu, *Small*, 2014, **10**, 4293–4297.

18 J. Song, F. Wu, Y. Wan and L. Ma, *Food Control*, 2015, **50**, 356–361.

19 A. Kumar, M. Bhatt, G. Vyas, S. Bhatt and P. Paul, *ACS applied materials & interfaces*, 2017, **9**, 17359–17368.

20 N. Ratnarathorn, O. Chailapakul and W. Dungchai, *Talanta*, 2015, **132**, 613–618.

21 V. V. Apyari, V. V. Arkhipova, A. I. Isachenko, P. A. Volkov, S. G. Dmitrienko and I. I. Torocheshnikova, *Sensors and Actuators B: Chemical*, 2018, **260**, 953–961.

22 D. Zhao, C. Chen, L. Lu, F. Yang and X. Yang, *Analyst*, 2015, **140**, 8157–8164.

23 P. J. Rivero, E. Ibañez, J. Goicoechea, A. Urrutia, I. R. Matias and F. J. Arregui, *Sensors and Actuators B: Chemical*, 2017, **251**, 624–631.

24 D. Sodzel, V. Khranovskyy, V. Beni, A. P. Turner, R. Viter, M. O. Eriksson, P.-O. Holtz, J.-M. Janot, M. Bechelany, S. Balme *et al.*, *Microchimica Acta*, 2015, **182**, 1819–1826.

25 F. Ghasemi, M. R. Hormozi-Nezhad and M. Mahmoudi, *Analytica chimica acta*, 2015, **882**, 58–67.

26 N. Fahimi-Kashani and M. R. Hormozi-Nezhad, *Analytical chemistry*, 2016, **88**, 8099–8106.

27 H. Rao, H. Ge, X. Wang, Z. Zhang, X. Liu, Y. Yang, Y. Liu, W. Liu, P. Zou and Y. Wang, *Microchimica Acta*, 2017, **184**, 3017–3025.

28 W. Sun, Y. Lu, J. Mao, N. Chang, J. Yang and Y. Liu, *Analytical chemistry*, 2015, **87**, 3354–3359.

29 A. R. Ferhan, L. Guo, X. Zhou, P. Chen, S. Hong and D.-H. Kim, *Analytical chemistry*, 2013, **85**, 4094–4099.

30 V. V. Apyari, S. G. Dmitrienko and Y. A. Zolotov, *Sensors and Actuators B: Chemical*, 2013, **188**, 1109–1115.

31 V. Arkhipova, V. Apyari and S. Dmitrienko, *Moscow University Chemistry Bulletin*, 2015, **70**, 28–33.

32 V. V. Apyari, V. V. Arkhipova, M. V. Gorbunova, P. A. Volkov, A. I. Isachenko, S. G. Dmitrienko and Y. A. Zolotov, *Talanta*, 2016, **161**, 780–788.

33 Y. Yang, Y.-Q. Li, S.-Y. Fu and H.-M. Xiao, *The Journal of Physical Chemistry C*, 2008, **112**, 10553–10558.

34 Y. Zhao, R.-J. Tong, M.-Q. Chen and F. Xia, *IEEE Photonics Technology Letters*, 2017, **29**, 1544–1547.

35 R. Tanimoto, T. Hiraiwa, Y. Nakai, Y. Shindo, K. Oka, N. Hiroi and A. Funahashi, *Scientific reports*, 2016, **6**, 22071.

36 H. Wang, A. Yang, Z. Chen and Y. Geng, *Optics and Spectroscopy*, 2014, **117**, 235–239.

37 T.-W. Sung and Y.-L. Lo, *Sensors and Actuators B: Chemical*, 2012, **173**, 406–413.

38 S. Kalytchuk, K. Polakova, Y. Wang, J. P. Froning, K. Cepe, A. L. Rogach and R. Zboril, *ACS nano*, 2017, **11**, 1432–1442.

39 Z. Zou, T. Wu, H. Lu, Y. Tu, S. Zhao, S. Xie, F. Han and S. Xu, *RSC Advances*, 2018, **8**, 7679–7686.

40 C. D. Brites, P. P. Lima, N. J. Silva, A. Millán, V. S. Amaral, F. Palacio and L. D. Carlos, *Nanoscale*, 2012, **4**, 4799–4829.

41 L. Shang, F. Stockmar, N. Azadfar and G. U. Nienhaus, *Angewandte Chemie International Edition*, 2013, **52**, 11154–11157.

42 H. Wang, F. Ke, A. Mararenko, Z. Wei, P. Banerjee and S. Zhou, *Nanoscale*, 2014, **6**, 7443–7452.

43 S. Lim, S. Gunasekaran and J.-Y. Imm, *Journal of food science*, 2012, **77**, N45–N49.

44 W. J. Kennedy, K. A. Slinker, B. L. Volk, H. Koerner, T. J. Godar, G. J. Ehlert and J. W. Baur, *ACS applied materials & interfaces*, 2015, **7**, 27624–27631.

45 W. J. Kennedy, S. N. Izor, B. Anderson, G. Frank, V. Varshney and G. J. Ehlert, *ACS applied materials & interfaces*, 2018.

46 X. Wang, Q. Liu, Y. Bu, C.-S. Liu, T. Liu and X. Yan, *Rsc Advances*, 2015, **5**, 86219–86236.

47 P. Mahata, S. K. Mondal, D. K. Singha and P. Majee, *Dalton Transactions*, 2017, **46**, 301–328.

48 E. J. McLaurin, L. R. Bradshaw and D. R. Gamelin, *Chemistry of Materials*, 2013, **25**, 1283–1292.

49 Y. Tian, Y. Tian, P. Huang, L. Wang, Q. Shi *et al.*, *Chemical Engineering Journal*, 2016, **297**, 26–34.

50 D. Chen, M. Xu and P. Huang, *Sensors and Actuators B: Chemical*, 2016, **231**, 576–583.

51 M. K. Mahata, T. Koppe, T. Mondal, C. Brüsewitz, K. Kumar, V. K. Rai, H. Hofsäss and U. Vetter, *Physical Chemistry Chemical Physics*, 2015, **17**, 20741–20753.

52 Q. Shao, Z. Yang, G. Zhang, Y. Hu, Y. Dong and J. Jiang, *ACS Omega*, 2018, **3**, 188–197.

53 X. Yang, Z. Fu, Y. Yang, C. Zhang, Z. Wu and T. Sheng, *Journal of the American Ceramic Society*, 2015, **98**, 2595–2600.

54 Y. Tian, B. Tian, P. Huang, L. Wang, B. Chen *et al.*, *Rsc Advances*, 2015, **5**, 14123–14128.

55 G. Jiang, S. Zhou, X. Wei, Y. Chen, C. Duan, M. Yin, B. Yang and W. Cao, *RSC Advances*, 2016, **6**, 11795–11801.

56 L. Marciniak, K. Prorok, L. Frances-Soriano, J. Perez-Prieto and A. Bednarkiewicz, *Nanoscale*, 2016, **8**, 5037–5042.

57 M. Hernández-Rodriguez, A. Lozano-Gorrín, V. Lavín, U. Rodríguez-Mendoza, I. Martín and F. Manjón, *Journal of Luminescence*, 2018.

58 J. Cao, X. Li, Z. Wang, Y. Wei, L. Chen and H. Guo, *Sensors and Actuators B: Chemical*, 2016, **224**, 507–513.

59 J. Cao, F. Hu, L. Chen, H. Guo, C. Duan and M. Yin, *Journal of Alloys and Compounds*, 2017, **693**, 326–331.

60 M. Runowski, A. Shyichuk, A. Tyminski, T. Grzyb, V. Lavín and S. Lis, *ACS applied materials & interfaces*, 2018, **10**, 17269–17279.

61 H. Li, Y. Zhang, L. Shao, Y. Wu, Z. Htwe and P. Yuan, *Optical Materials*, 2017, **69**, 238–243.

62 D. Wawrzynczyk, A. Bednarkiewicz, M. Nyk, W. Strek and M. Samoc, *Nanoscale*, 2012, **4**, 6959–6961.

63 S. Zheng, W. Chen, D. Tan, J. Zhou, Q. Guo, W. Jiang, C. Xu, X. Liu and J. Qiu, *Nanoscale*, 2014, **6**, 5675–5679.

64 E. Hertle, L. Chepyga, M. Batentschuk, S. Will and L. Zigan, *Journal of Luminescence*, 2018, **204**, 64–74.

65 X. Wang, Y. Wang, J. Yu, Y. Bu and X. Yan, *Optics express*, 2018, **26**, 21950–21959.

66 S. Arai, S. Takeoka, S. Ishiwata, H. Sato, M. Suzuki *et al.*, *Analyst*, 2015, **140**, 7534–7539.

67 F. Ye, C. Wu, Y. Jin, Y.-H. Chan, X. Zhang and D. T. Chiu, *Journal of the American Chemical Society*, 2011, **133**, 8146–8149.

68 H. Sun, M. Yu, X. Sun, G. Wang and J. Lian, *The Journal of Physical Chemistry C*, 2013, **117**, 3366–3373.

69 S. P. Danielsen, J. Choi and R. J. Composto, *Journal of Polymer Science Part B: Polymer Physics*, 2016, **54**, 301–307.

70 D. Nepal, K. Park and R. A. Vaia, *Small*, 2012, **8**, 1013–1020.

71 N. A. Joy, B. K. Janiszewski, S. Novak, T. W. Johnson, S.-H. Oh, A. Raghunathan, J. Hartley and M. A. Carpenter, *The Journal of Physical Chemistry C*, 2013, **117**, 11718–11724.

72 S. Maity, W.-C. Wu, C. Xu, J. B. Tracy, K. Gundogdu, J. R. Bochinski and L. I. Clarke, *Nanoscale*, 2014, **6**, 15236–15247.

73 S. Schnell and T. E. Turner, *Progress in Biophysics and Molecular Biology*, 2004, **85**, 235–260.

74 K. Luby-Phelps, in *International Review of Cytology*, ed. H. Walter, D. E. Brooks and P. A. Srere, Academic Press, 1999, vol. 192 of Microcompartmentation and Phase Separation in Cytoplasm, pp. 189–221.

75 B. D. Allen, A. C. Benniston, A. Harriman, S. A. Rostron and C. Yu, *Physical Chemistry Chemical Physics*, 2005, **7**, 3035–3040.

76 S. Raut, J. Kimball, R. Fudala, H. Doan, B. Maliwal, N. Sabnis, A. Lacko, I. Gryczynski, S. V. Dzyuba and Z. Gryczynski, *Physical Chemistry Chemical Physics*, 2014, **16**, 27037–27042.

77 X. Peng, Z. Yang, J. Wang, J. Fan, Y. He, F. Song, B. Wang, S. Sun, J. Qu, J. Qi and M. Yan, *Journal of the American Chemical Society*, 2011, **133**, 6626–6635.

78 A. A. Bhagwat, D. R. Mohbiya, K. C. Avhad and N. Sekar, *Spectrochimica Acta Part A: Molecular and Biomolecular Spectroscopy*, 2018, **203**, 244–257.

79 R. Kotani, H. Sotome, H. Okajima, S. Yokoyama, Y. Nakaike, A. Kashiwagi, C. Mori, Y. Nakada, S. Yamaguchi, A. Osuka, A. Sakamoto, H. Miyasaka and S. Saito, *Journal of Materials Chemistry C*, 2017, **5**, 5248–5256.

80 W. Chen, C. Gao, X. Liu, F. Liu, F. Wang, L.-J. Tang and J.-H. Jiang, *Analytical Chemistry*, 2018, **90**, 8736–8741.

81 M. A. Haidekker, W. J. Akers, D. Fischer and E. A. Theodorakis, *Optics Letters*, 2006, **31**, 2529–2531.

82 M. A. Haidekker and E. A. Theodorakis, *Journal of Biological Engineering*, 2010, **4**, 11.

83 M. K. Kuimova, G. Yahioglu, J. A. Levitt and K. Suhling, *Journal of the American Chemical Society*, 2008, **130**, 6672–6673.

84 J. A. Levitt, M. K. Kuimova, G. Yahioglu, P.-H. Chung, K. Suhling and D. Phillips, *The Journal of Physical Chemistry C*, 2009, **113**, 11634–11642.

85 M. A. Haidekker, T. P. Brady, D. Lichlyter and E. A. Theodorakis, *Journal of the American Chemical Society*, 2006, **128**, 398–399.

86 Z. Yang, Y. He, J.-H. Lee, N. Park, M. Suh, W.-S. Chae, J. Cao, X. Peng, H. Jung, C. Kang and J. S. Kim, *Journal of the American Chemical Society*, 2013, **135**, 9181–9185.

87 J. E. Chambers, M. Kubánková, R. G. Huber, I. López-Duarte, E. Avezov, P. J. Bond, S. J. Marciniak and M. K. Kuimova, *ACS Nano*, 2018, **12**, 4398–4407.

88 R. Ghosh, A. Kushwaha and D. Das, *The Journal of Physical Chemistry B*, 2017, **121**, 8786–8794.

89 F. Zhou, J. Shao, Y. Yang, J. Zhao, H. Guo, X. Li, S. Ji and Z. Zhang, *European Journal of Organic Chemistry*, 2011, **2011**, 4773–4787.

90 T. Liu, X. Liu, D. R. Spring, X. Qian, J. Cui and Z. Xu, *Scientific Reports*, 2014, **4**, 5418.

91 A. Mustafic, K. M. Elbel, E. A. Theodorakis and M. Haidekker, *Journal of Fluorescence*, 2015, **25**, 729–738.

92 J. Mei, Y. Hong, J. W. Y. Lam, A. Qin, Y. Tang and B. Z. Tang, *Advanced Materials*, 2014, **26**, 5429–5479.

93 S. Chen, Y. Hong, Y. Zeng, Q. Sun, Y. Liu, E. Zhao, G. Bai, J. Qu, J. Hao and B. Z. Tang, *Chemistry – A European Journal*, 2015, **21**, 4315–4320.

94 M. A. Correa-Duarte, V. Salgueiriño-Maceira, A. Rinaldi, K. Sieradzki, M. Giersig and L. M. Liz-Marzán, *Gold Bulletin*, 2007, **40**, 6–14.

95 L. Fu, Y. Liu, W. Wang, M. Wang, Y. Bai, E. L. Chronister, L. Zhen and Y. Yin, *Nanoscale*, 2015, **7**, 14483–8.

96 D. A. Davis, A. Hamilton, J. Yang, L. D. Cremar, D. Van Gough, S. L. Potisek, M. T. Ong, P. V. Braun, T. J. Martinez, S. R. White, J. S. Moore and N. R. Sottos, *Nature*, 2009, **459**, 68–72.

97 C. A. S. Burel, A. Alsayed, L. Malassis, C. B. Murray, B. Donnio and R. Dreyfus, *Small*, 2017, **13**, year.

98 S. N. Raja, D. Zherebetskyy, S. Wu, P. Ercius, A. Powers, A. C. Olson, D. X. Du, L. Lin, S. Govindjee, L. W. Wang, T. Xu, A. P. Alivisatos and R. O. Ritchie, *Nano Lett*, 2016, **16**, 5060–7.

99 S. N. Raja, X. Ye, M. R. Jones, L. Lin, S. Govindjee and R. O. Ritchie, *Nat Commun*, 2018, **9**, 1155.

100 K. C. Avhad, D. S. Patil, S. Chitrambalam, M. C. Sreenath, I. H. Joe and N. Sekar, *Optical Materials*, 2018, **79**, 90–107.

101 H. Zhu, J. Fan, J. Du and X. Peng, *Accounts of Chemical Research*, 2016, **49**, 2115–2126.

102 F. Hild and S. Roux, *Strain*, 2006, **42**, 69–80.

103 B. Pan, K. Qian, H. Xie and A. Asundi, *Measurement science and technology*, 2009, **20**, 062001.

104 D. Ryu, K. J. Loh, R. Ireland, M. Karimzada, F. Yaghmaie and A. M. Gusman, *Smart Structures and Systems*, 2011, **8**, 471–486.

105 T. Maurer, J. Marae-Djouda, U. Cataldi, A. Gontier, G. Montay, Y. Madi, B. Panicaud, D. Macias, P.-M. Adam, G. Lévêque, T. Bürgi and R. Caputo, *Frontiers of Materials Science*, 2015, **9**, 170–177.

106 U. Cataldi, R. Caputo, Y. Kurylyak, G. Klein, M. Chekini, C. Umeton and T. Bürgi, *J. Mater. Chem. C*, 2014, **2**, 7927–7933.

107 M. G. Millyard, F. Min Huang, R. White, E. Spigone, J. Kivioja and J. J. Baumberg, *Applied Physics Letters*, 2012, **100**, 073101.

108 L. Minati, A. Chiappini, F. Benetti, G. Speranza, D. Zonta, A. Piotrowska, M. Marciniak, A. Vaccari and M. Ferrari, *Colloids and Surfaces A: Physicochemical and Engineering Aspects*, 2015, **482**, 431–437.

109 M. Böhm, T. Uhlig, S. Derenko and L. M. Eng, *Optical Materials Express*, 2017, **7**, 1882.

110 T. Sannomiya, C. Hafner and J. Vörös, *Optics Letters*, 2009, **34**, 2009.

111 C. Minnai and P. Milani, *Applied Physics Letters*, 2015, **107**, 073106.

112 B. C. Marin, J. Liu, E. Aklile, A. D. Urbina, A. S. Chiang, N. Lawrence, S. Chen and D. J. Lipomi, *Nanoscale*, 2017, **9**, 1292–1298.

113 K. B. Ford, M. K. Collins, N. E. Ajami, D. Dowds, K. Mesyef, J. Trovillion, G. Al-Chaar and C. P. Marsh, *Materials Letters*, 2013, **106**, 301–303.

114 S. F. Yin, Z. M. Zhao, W. L. Luan and S. T. Tu, *Procedia Engineering*, 2015, **130**, 1788–1794.

115 C. L. Choi, K. J. Koski, A. C. Olson and A. P. Alivisatos, *Proc Natl Acad Sci U S A*, 2010, **107**, 21306–10.

116 L. S. Fu, W. S. Wang, C. Y. Xu, Y. Li and L. Zhen, *Sci Rep*, 2017, **7**, 1676.

117 C. J. Orendorff, S. C. Baxter, E. C. Goldsmith and C. J. Murphy, *Nanotechnology*, 2005, **16**, 2601–2605.

118 K. Jia, X. He, X. Zhou, D. Zhang, P. Wang, Y. Huang and L. Xiaobo, *Sensors and Actuators B: Chemical*, 2018, **257**, 442–450.

119 T. Fischer, S. Stottinger, G. Hinze, A. Bottin, N. Hu and T. Basche, *Nano Lett*, 2017, **17**, 1559–1563.

120 L. Fang, J. Y. Park, Y. Cui, P. Alivisatos, J. Shcrier, B. Lee, L.-W. Wang and M. Salmeron, *The Journal of Chemical Physics*, 2007, **127**, 184704.

121 S. N. Raja, A. C. Olson, K. Thorkelsson, A. J. Luong, L. Hsueh, G. Chang, B. Gludovatz, L. Lin, T. Xu, R. O. Ritchie and A. P. Alivisatos, *Nano Lett*, 2013, **13**, 3915–22.

122 X. Jin, M. Gotz, S. Wille, Y. K. Mishra, R. Adelung and C. Zollfrank, *Adv Mater*, 2013, **25**, 1342–7.

123 F. Cellini, L. Zhou, S. Khapli, S. D. Peterson and M. Porfiri, *Mechanics of Materials*, 2016, **93**, 145–162.

124 H. Shou, K. Jia, X. Zhou, L. Gao, X. He, X. Zhou, D. Zhang and X. Liu, *Journal of Materials Chemistry C*, 2017, **5**, 4134–4138.

125 J. W. Woodcock, R. Beams, C. S. Davis, N. Chen, S. J. Stranick, D. U. Shah, F. Vollrath and J. W. Gilman, *Advanced Materials Interfaces*, 2017, **4**, 1601018.

126 G. Yeroslavsky, M. Kamimura, R. Inoue, Y. Kogo and K. Soga, *Journal of Photopolymer Science and Technology*, 2018, **31**, 533–540.

127 G. A. Filonenko and J. R. Khusnutdinova, *Advance Materials*, 2017, **29**, 1700563.

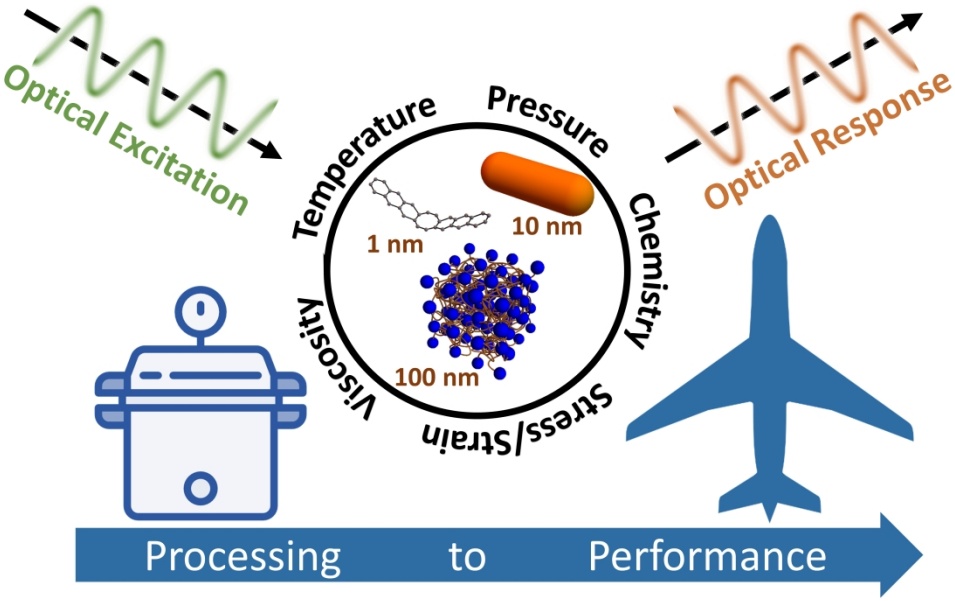
Optical Excitation
Temperature
Pressure
Chemistry
Stress/Strain
Viscosity
1 nm
10 nm
100 nm
Optical Response
Processing to Performance

We provide a broad review of optically responsive materials with potential for in-situ monitoring of material state properties in structural polymer-based materials with nanoscale spatial resolution.